ROMANIAN ACADEMY
Doctoral School of Chemical Sciences
„Petru Poni" Institute of Macromolecular Chemistry
CHEMISTRY field

SUMMARY OF DOCTORAL THESIS

NEW APPROACHES FOR THE DEVELOPMENT OF FUNCTIONALIZED POLYMER NANOSYSTEMS WITH APPLICATIONS IN NANOMEDICINE

Scientific Coordinator:
C.S. I, PhD Mariana PINTEALĂ

PhD Student:
Răzvan GHIARASIM

2024

Mrs/Mr. ....

We inform you that on **9ᵗʰ of April 2024**, **11 am**, in the **"Petru Poni" Institute of Macromolecular Chemistry**, Iasi, will take place the public presentation of the doctoral thesis *"New approaches for the development of functionalized polymeric nanosystems with applications in nanomedicine"*, author **Răzvan Ghiarasim**, in order to confer the scientific title of doctor.

PRESIDENT:

CS I Dr Valeria Harabagiu

"Petru Poni" Institute of Macromolecular Chemistry, Iasi

DOCTORAL SUPERVISOR:

CS I Dr. Mariana Pinteală

"Petru Poni" Institute of Macromolecular Chemistry, Iasi

REFEREES:

Prof. Dr. Adrian Covic

"Gr. T. Popa "University of Medicine and Pharmacy, Iasi

Prof. Dr. Ionel Mangalagiu

Alexandru Ioan Cuza University of Iasi

Dr. Habil. Marcela Mihai

"Petru Poni" Institute of Macromolecular Chemistry ", Iasi

In accordance with the Regulation on the organization and conduct of the doctorate for the granting of scientific titles in the Romanian Academy, we send you the summary of the doctoral thesis with the request to communicate your appreciations and observations. On this occasion, we invite you to participate in the public defense of your doctoral thesis.

Director,

Dr. Valeria Harabagiu

Acknowledgements

This doctoral thesis marks the conclusion of a significant stage in my professional evolution, and on this occasion, I would like to express my sincere gratitude to the people who guided, supported, and guided me during the years of doctoral studies, thus contributing to the elaboration and completion of this doctoral thesis.

My sincerest and deepest thanks to the **C.S. I Dr. Mariana Pinteală** for the opportunity to be part of an exceptional team and laboratory, which represented the favourable environment for scientific research and contributed significantly to my personal evolution. I am grateful for his constant guidance and support during this period. The result of this remarkable collaboration is reflected in this doctoral thesis.

I would like to express my special gratitude to the **C.S. II Dr. Alexandru Rotaru** for the exemplary patience and perseverance manifested in my guidance as a young researcher, as well as for the generous support granted throughout the elaboration and completion of the doctoral thesis.

Special thanks to colleagues from **IntelCenter** for their direct contributions to the elaboration of this thesis. I would also like to express my appreciation to my colleagues from the departments **Institute of Macromolecular Chemistry "Petru Poni"** who have made significant contributions to the physicochemical analyses required during my PhD internship.

I would like to express my sincere thanks **Romanian Academy** and **"Petru Poni" Institute of Macromolecular Chemistry** for the opportunity to carry out the doctoral internship within the Institute and for the access to its infrastructure, which were essential in successfully achieving all the proposed objectives.

I would like to express my gratitude to the projects „**ModNanoMPol**" PN-III-P1-1.1-TE-2019-0922 and „**NanoHER2Restore**" EEA-RO-NO-2018-0246, for financial support granted during doctoral studies.

Finally, I would like to thank them **my family** for all the moral and financial support given in recent years.

Thank you!
PhD student Răzvan Ghiarasim

TABLE OF CONTENT

INTRODUCTION

According to the Institute for Health Measurement and Evaluation (IHME), cancer is currently the biggest health problem globally, causing one in six deaths worldwide. Conventional cancer treatments, such as surgery, radiation therapy and chemotherapy, currently have limitations, with the risk of causing damage to healthy tissues or failing to ensure complete eradication of tumours. Research into cancer therapy using nanotechnology goes beyond the mere delivery of medicines, being extended to the development of new treatments only through the characteristics of nanomaterials themselves. First, certain physical properties of nanoparticles, such as energy absorption and re-emission, can be used to affect diseased tissues, as can be seen in applications of laser ablation and hyperthermia. Secondly, nanoparticles are small enough (on the order of tens of nanometres) to accumulate in cancer areas, but large enough to be able to charge many therapeutic compounds, such as radionuclides or biologically active molecules. Third, the generous surface area of these nanoparticles can be functionalized with ligands, such as strands of DNA, RNA, peptides, or antibodies, which can actively guide nanoparticles throughout the body. These properties of nanoparticles facilitate efficient drug delivery and lead to improved multimodal and theranostic therapies (Arruebo et al., 2011; Schena, Saccomandi and Fong, 2017; Crezee, Franken and Oei, 2021; Poletto et al., 2022; Jahangirian et al., 2019;Singh et al., 2020; Sharma et al., 2022; Marega et al., 2012).

Starting from the fact that nanomedicine represents a promising direction for innovation in the medical field, especially in cancer treatment, the present doctoral thesis, entitled **"New approaches for the development of functionalized polymeric nanosystems with applications in nanomedicine"**, It aimed to obtain, physico-chemical characterization and demonstrate the applicability in cancer treatment of two types of synthetic chemical nanosystems based on biocompatible polymers, which were subsequently functionalized with different biologically active molecules, both small molecular compounds and proteins.

The thesis is divided into two well-formulated parts, each highlighting specific objectives. **First part** of the thesis focuses on **Chapter I**, where a literature study is presented on nanoparticles used in cancer therapy, both those approved by Food and Drug Administration (FDA) and the European Medicines Agency (EMA), as well as those in the approval stages.

Part Two of that sentence (**Chapter II** and **III**) builds on personal contributions resulting from the development of two types of nanosystems (magnetic nanoparticles and copolymer micelles) with applications in cancer therapy. Each chapter begins with the presentation of specific objectives, motivation for choosing the studied systems,

physicochemical characterization, applications *in vitro*, and conclusions drawn from their own experimental data.

Chapter II It comprises two subchapters presenting two studies based on the development of magnetic nanoparticles decorated with methacrylate polymers and subsequently functionalized with low molecular weight biologically active molecules (folic acid and methotrexate).

In Subchapter II.2 the synthesis of magnetic nanoparticles by coprecipitation method is described, followed by their functionalization with a polymerization initiator specific to atom transfer radical polymerization (ATRP). The initiator allowed polymerization of the monomer 2-hydroxyethyl methacrylate (HEMA), by surface-initiated atom transfer radical polymerization mechanism (SI-ATRP), resulting in polymeric chains of poly(2-hydroxyethyl methacrylate) (PHEMA) grafted onto the surface of magnetic nanoparticles. After this step, the PHEMA chains were functionalized with folic acid (FA), which is the targeting unit of cancer cells. Through this process, two types of magnetic nanoparticles decorated with functionalized PHEMA chains with different concentrations of FA were obtained. All synthesis steps of this study, including the synthesis of non-functionalized nanoparticles, those with surface polymerization initiator, those with polymers and nanoparticles subsequently decorated with functionalized polymers with FA, were characterized using different physicochemical techniques, such as FTIR, TGA/DTG, DSC, TEM, STEM and DLS. The FA concentration was quantified by UV-Vis spectroscopy using the calibration curve method. The cell viability of the nanoparticles was assessed on one normal cell line (NHDF) and three cancer cell lines (MCF-7, HeLa and HepG2). The results obtained indicated that the synthesized nanoparticles are biocompatible on all four cell lines. The notable difference between these cell lines was that FA-functionalized nanoparticles were internalized in a higher concentration by cancer cells due to overexpression of folate receptors on their surface compared to normal cells. This result was confirmed by measuring the concentration of intracellular iron after incubation of cells with nanoparticles using the thiocyanate method. It has also been shown that an increase in the concentration of FA used to functionalised nanoparticle surfaces led to greater internalisation of nanoparticles. This observation was also confirmed by the determination of intracellular iron concentration by atomic absorption spectrometry. In addition, in this study, the use of these nanoparticles in magnetic resonance imaging was highlighted.

Subchapter II.3 focuses on the study of polymerization, by SI-ATRP mechanism, of three methacrylate-type monomers (HEMA, PEGMA6, PEGMA10), using the same system of nanoparticles decorated with the ATRP initiator from the first study of this chapter. This process

was followed by functionalization of polymer chains with a folic acid antimetabolite called methotrexate (MTX). As in the case of nanoparticles obtained in subchapter II.2, the synthesis steps of these nanoparticles have been characterization using various physicochemical techniques. The quantification of MTX was performed by UV-Vis spectroscopy, using the calibration curve method. In this study, we chose to use MTX because of its properties, such as its ability to bind specifically to folate receptors and its therapeutic effect by inhibiting an enzyme involved in cell division. MTX-functionalized nanoparticles were found to be biocompatible on human gingival fibroblasts (HGF) and showed higher toxicity on the MCF-7 cell line, compared to free drug at the same concentrations of MTX.

These results highlight the versatility of grafting methacrylate-type polymers with different molar masses of monomer units onto a spherical surface and the impact of the length of these units on MTX functionalization and increased cytotoxicity on the MCF-7 cancer cell line.

Chapter III presents two supramolecular assembly studies of nanostructured entities, one based on the development of a micelle-type system with the property of controlled drug release in the extracellular cancer environment (Subchapter III.3) and the second (Subchapter III.4) based on the functionalization of these micelles with a monoclonal antibody, which leads to increased therapeutic effect on cancer cell lines specific to breast cancer.

Thus, in Subchapter III.3, three polyethylene glycol-polyhistidine (PEG-PHis) copolymers with a molecular weight of 2 kDa and three different PHis lengths (20, 26 and 32 histidine monomer units) were obtained, applying the technique: solid support peptide synthesis (SPPS). For these three copolymers, critical micelles concentrations were determined by fluorescence spectroscopy, using pyrene as the model fluorescent compound. The copolymers were then assembled into corresponding unloaded micelles and loaded with doxorubicin (DOX), a therapeutic model compound, to show that these micelles release the drug within the pH range of the extracellular cancer environment (7.2 to 6.5). The micelles obtained were dimensionally characterized by DLS and morphological analysis was highlighted by STEM. The controlled release of DOX from micelles was evidenced by fluorescence studies conducted in PBS at three different pH values. Cell viability tests on a specific breast cancer line (MDA-MB-231) concluded that DOX was released controlled over 72 hours and resulted in a controlled decrease in cell viability over the free drug. In addition, the developed micelles can release the drug in a narrow pH range, namely between 7.2 and 6.5, which represents the pH of the extracellular cancer environment. The development of this type of micelles can help

transport other specific active principles to cancer cells and release them on the cell surface where, in most cases, receptors specific to these principles are found.

In Subchapter III.4 PEG-PHis micelles were functionalized in a controlled manner with a monoclonal antibody called trastuzumab (Tzm), specifically for inhibiting the HER2 transmembrane glycoprotein receptor involved in cell growth, overexpressed in breast cancer-specific cancer cells. Thus, the micelles of non-functionalized preparations and those functionalized with Tzm were analysed from a physicochemical point of view by DLS, NTA and STEM. Their stability was determined by exposing them to a concentration of BSA simulating the total concentration of proteins in human serum, so the non-functionalized ones were completely destabilized, while those functionalized with Tzm remained stable for a period of 72 hours. The micelles were biocompatible on the normal HGF cell line, but in the case of three breast cancer-specific cancer cell lines (MDA-MB-361, SK-BR-3, BT-474), when the Tzm was covalently bound to the micelle surface, cell viability decreased significantly compared to non-functionalized micelles and free Tzm. This decrease was observed in both 2D and 3D cell cultures (spheroids).

The doctoral thesis ends with a series of general conclusions from each study carried out, the dissemination of the results during the doctoral studies and finally the bibliographic references related to the thesis.

PART II - Personal contributions

CHAPTER II - Magnetic nanoparticles decorated with methacrylate polymers functionalized with bioactive molecules

II.1. Motivation and objectives of the Chapter II study

II.1.1. Specific scientific objectives:

I. Synthesis and characterization of magnetic nanoparticles.

II. Synthesis and characterization of an ATRP-type polymerisation initiator and its covalent binding to the surface of magnetic nanoparticles synthesized in step I.

III. PHEMA grafting, by means of the SI-ATRP polymerization mechanism, using magnetic nanoparticles functionalized with polymerization initiator specific to the ATRP mechanism, synthesized in stage II.

IV. Functionalization of nanoparticles obtained in step III with folic acid in various concentrations.

V. Conducting *in vitro* studies of functionalized magnetic nanoparticles obtained in stage IV on normal dermal fibroblasts (NHDF) and cancer cell lines (MCF-7, HeLa and HepG2). The aim was to evaluate biocompatibility, cytotoxicity and cellular uptake capacity depending on folic acid concentration of synthesized nanoparticles. Nuclear magnetic resonance imaging studies have also been provided.

VI. Grafting of three methacrylate polymers by means of the SI-ATRP polymerization mechanism, using functionalized magnetic nanoparticles with polymerization initiator specific to the ATRP mechanism synthesized in step II.

VII. Functionalization with methotrexate (MTX) of nanoparticles synthesized in step VI.

VIII. Determination of cell viability of systems obtained in stage VII on a normal cell line (HGF) and a cancer cell line (MCF-7).

II.1.2. The motivation for the choice of magnetic nanoparticles and methacrylate polymers

A potentially real direction for clinical applicability and that has been well studied over the past two decades is based on magnetic nanoparticles (MNPs), a class of metal oxides capable of being oriented and even accumulated in desired tissue through an external magnetic field. Furthermore, MNPs can be coated, functionalized, and loaded with therapeutic substances to be transported and released in a controlled manner to a studied target. The mentioned systems may exhibit good colloidal stability, high biocompatibility, low cytotoxicity, non-immunogenicity, increased circulation time in the blood and finally may exhibit a high loading, transport, and controlled delivery capacity to a drug target under physiological conditions. Furthermore, MNPs can be used in cancer screening and diagnosis as contrast agents for magnetic resonance imaging (MRI). So far, the most studied contrast agents have been Fe^{3+}-based (Anghelache et al., 2021; Lungoci et al., 2019; Beagan et al., 2020), superparamagnetic iron oxide (SPION) nanoparticles, which showed an increase in contrast in transverse relaxation (T2). MNPs were functionalized with different types of molecular fragments, as well as macromolecular compounds, without affecting their characteristics in the functionalization process. Especially important is their functionalization with polymers that can provide specific properties depending on their nature. Two strategies are currently used to synthesize hybrid materials based on polymer-coated nanoparticles: (I) physical adsorption of polymers on the surface of uncoated MNPs (Bregoli et al., 2016) and (II) covalent grafting of polymers onto the surface of inorganic nanomaterials by three methods: (a) grafting-to, (b) grafting-from, and (c) grafting through. The polymers used to graft the surface of nanoparticles can most commonly

be obtained by ATRP polymerization (atomic transfer radical polymerization), where the most used monomers are acrylic ones, such as N,N-dimethyl aminoethyl methacrylate, oligo methacrylate (ethylene glycol) methyl ether and poly(ethylene glycol) methacrylate. These monomers have been successfully used to decorate magnetic nanoparticles with grafted polymers with various functions that are able to interact with different biologically active molecules (e.g. folic acid and methotrexate) for the development of nanocarriers capable of interacting with specific receptors on the surface of targeted cells, ensuring drug delivery to the target cell (Israel et al., 2020; Sung and Kim, 2020; Baek et al., 2015).

II.2. Results and discussion
II.2.1. Magnetic nanoparticles decorated with folic acid functionalized PHEMA chains
II.2.1.1. The motivation for the choice of PHEMA polymer and folic acid

The polymer poly(2-hydroxyethyl methacrylate) (PHEMA), obtained by ATRP polymerization of the monomer 2-hydroxyethyl methacrylate (HEMA), has recently attracted interest due to the hydroxyl groups (-OH) present on each monomer unit. These groups can be converted into carboxylic groups (-COOH) and functionalized with specific molecules to improve bioactivity or initiate cycle-opening radical polymerization. PHEMA also exhibits properties such as increased hydrophilicity and biocompatibility, being like polyethylene glycol (PEG) in terms of "non-fouling" properties (Beers et al., 1999). PHEMA chains retain their "non-fouling" properties even after functionalization with biologically active molecules. Functionalization of nanoparticles with targeting units, such as folic acid (FA), may allow specific binding to the surface of cancer cells because FA interacts with the overexpressed folate receptor (FAα) on these cells. FA has been successfully used to functionalize a wide range of chemical systems, including polymer-coated magnetic nanoparticles, liposomes, and hydrogels. These functionalization strategies can facilitate targeted drug delivery and improve therapy efficacy in cancer treatment.

The purpose of the study in **Subchapter II.2.1.** was to develop a functional nanosystem based on magnetic nanoparticles, decorated with PHEMA chains having the property of "non-fouling" with high specificity and the property of internalizing into cancer cells by functionalizing PHEMA with folic acid (a presentation of the synthesis steps for obtaining this nanosystem is presented in **scheme II.2**).
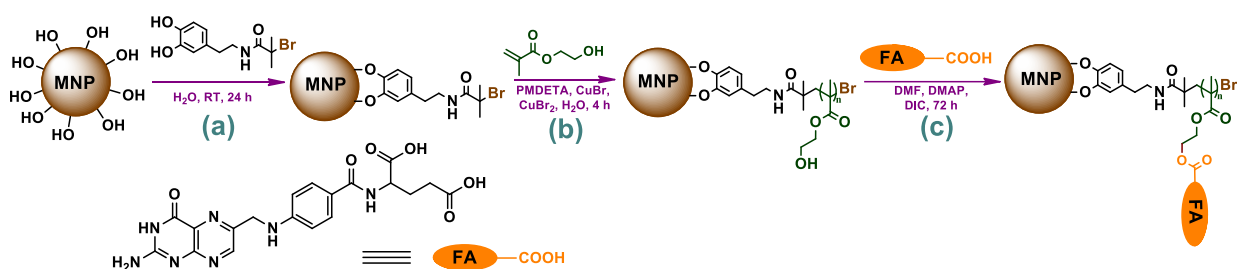
Scheme II.2. Synthesis steps to obtain the nanosystem: (a) grafting of the polymerisation initiator of ATRP type onto the surface of the nanoparticles, (b) polymerisation of the HEMA monomer by SI-ATRP and (c) functionalisation of PHEMA with FA (Ghiarasim et al., 2021).

In this study, initially, the capacity of folic acid-functionalized nanoparticles to internalize at a significantly higher concentration compared to normal cells was examined, concurrently with the increase in this internalization as the concentration of FA used for functionalization increased. Additionally, the potential of poly(hydroxyethyl methacrylate) (PHEMA)-decorated nanoparticles functionalized with FA as contrast agents in magnetic resonance imaging was demonstrated.

II.2.1.2. Synthesis and physicochemical characterization of magnetic nanoparticles decorated with PHEMA chains functionalized with folic acid

Non-functionalised magnetic nanoparticles (MNP-OH, **scheme II.2.**) were synthesized by coprecipitation of iron (II and III) chlorides in a basic medium, eventually yielding nanoparticles with free hydroxyl groups on the surface. Raman spectroscopy and XRD analysis were used to confirm the structure of these nanoparticles.

In parallel, the polymerisation initiator specific to radical polymerisation of a vinyl monomer by ATRP mechanism was synthesized by the reaction between L-dopamine and α-bromo butyl bromide according to **reaction scheme II.3**.
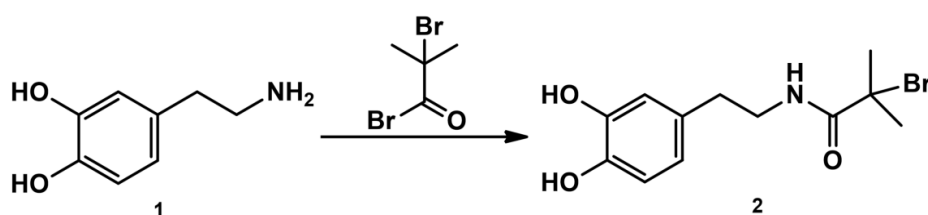
Scheme II.3. Synthesis of ATRP polymerization initiator (Ghiarasim et al., 2021).

The purity of initiator 2 was assessed by proton nuclear magnetic resonance spectroscopy (1H-NMR). Each synthesis step in **scheme II.2.** has been analysed physiochemically by techniques such as Fourier transform infrared spectroscopy (FTIR), thermogravimetric analysis (TGA), differential scanning calorimetry (DSC), determination of magnetic properties using a vibrating sample magnetometer (VSM), dynamic light diffusion (DLS). The most important technique for highlighting the obtaining of functionalized

nanoparticles was the FTIR technique (**figure II.3**.). FTIR spectrum of non-functionalised nanoparticles (MNP-OH) showed specific bands such as Fe-O bond at 561 cm^{-1} and hydroxyl groups at 3412 cm^{-1}. Binding of the ATRP initiator to the surface of nanoparticles (MNP-I) was confirmed by the appearance of bands characteristic of the initiator. Polymerisation of the HEMA monomer by SI-ATRP (**figure II.3.,** MNP-PHEMA-OH), resulted in the occurrence in the FTIR spectrum of bands at 2978 and 2885 cm^{-1} characteristic of the C-H bond vibration band in groups -CH$_3$ and -CH$_2$-, respectively, in the main polymer chain (PHEMA), one strip at 3421 cm^{-1} characteristic of the vibration band of the OH group in the repetitive monomer units of the PHEMA structure, an intense band at 1720 cm^{-1} characteristic of the C=O bond and the vibration bands at 1251, 1153 and 1076 cm^{-1} assigned to C-C, C-O and C-O-C bonds. And in the case

Figure II.3. FTIR spectra of MNP-OH, MNP-I, MNP-PHEMA-OH, MNP-PHEMA-FA1 and MNP-PHEMA-FA2 nanoparticles. The inserted image represents the wavelength range where the vibration band specific to the amide bond in the structure of folic acid used to functionalized PHEMA (MNP-PHEMA-FA1/2) is located (Ghiarasim et al., 2021).

of this sample, the preservation of the vibration band of the Fe-O bond can be observed in the FTIR spectrum. The presence of the polymer on the surface of the nanoparticles was also highlighted by the complete disappearance of the vibration band C=C from 1632 cm^{-1}, specific to the vinyl monomer HEMA (**figure II.3.**). Functionalisation with FA of PHEMA chains grafted onto the surface of nanoparticles (**figure II.3.**, MNP-PHEMA-FA1/2) is evidenced by the appearance of two bands characteristic of FA, such as that at 1604 cm^{-1} assigned to the vibration band of the C=C bond of the phenolic part and that at 1653 cm^{-1} characteristic of the amide bond (FTIR spectrum inserted in **figure II.3.**) (Liu et al., 2020).

Quantification of folic acid reacted with hydroxyl groups in PHEMA (MNP-PHEMA-OH) was performed by the calibration curve method using ultraviolet-visible (UV-Vis) spectroscopy. Analysing UV-Vis spectra from **figure II.4.a.**, it can be observed that MNP-OH

and MNP-PHEMA-OH samples show no major absorption bands in the ultraviolet-visible range, while magnetic nanoparticles decorated with FA-functionalized polymers (MNP-PHEMA-FA1/2) showed a 282 nm absorption band, specific to folic acid (free FA).
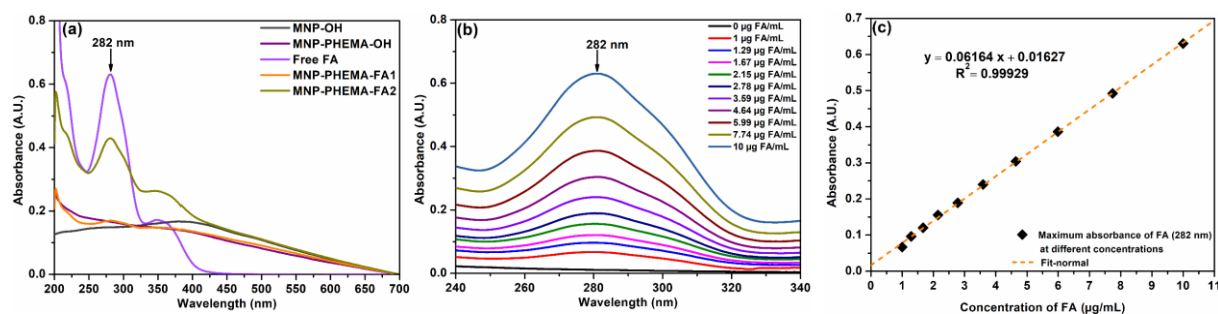
Figure II.4. (a) Ultraviolet visible (UV-Vis) absorption spectra of MNP-OH, MNP-PHEMA-OH, NPN-PHEMA-FA1 and MNP-PHEMA-FA2 nanoparticles and free FA, respectively; (b) absorption spectra of solutions of FA at different concentrations (0 to 10 μg FA/mL); (c) FA calibration curve. UV-Vis spectra were obtained by measuring absorbances of system solutions in PBS at pH = 7,4 (Ghiarasim et al., 2021) .

System-specific FA concentrations studied (**figure II.4.a.**) were determined using the calibration curve for FA (**figure II.4.c.**). The calibration curve was constructed by plotting the maximum absorption at 282 nm vs FA concentration of the data in **figure II.4.b**. Thus, FA concentrations in MNP-PHEMA-FA1 samples of 31.5 μg FA/mg sample and MNP-PHEMA-FA2 of 83.5 μg FA/mg sample were determined.

Regarding hydrodynamic diameters and information on colloidal stability in aqueous solutions of the studied nanoparticles, the technique called dynamic light diffusion (DLS) was used. In **figure II.8.a.** mean hydrodynamic diameters as a function of nanoparticle concentration in solution (1x PBS) of MNP-OH, MNP-I, MNP-PHEMA-OH, MNP-PHEMA-FA1 and MNP-PHEMA-FA2 samples shall be provided. Analysing the curves of the average hydrodynamic diameters in **figure II.8.a.**, an increase in nanoparticle concentrations leads to an increase in hydrodynamic diameters, indicating the formation of aggregates. The samples showed the smallest hydrodynamic diameters when the concentration was less than 50 μg/mL, the nanoparticles tend to be dispersed under these conditions, an important parameter for efficient use in biological tests.

By analysing variations in the zeta potentials of the nanoparticles (**figure II.8.b.**) depending on their concentration, it can be observed that MNP-OH, MNP-I samples show moderate colloidal stability over the entire concentration range. Decorating the surface of nanoparticles with PHEMA leads to high colloidal instability, but the introduction of FA increases the colloidal stability of the nanoparticles (increase observed for both FA concentrations). From a morphological point of view, transmission electron microscopy (TEM) was used to highlight the shape of nanoparticles and the measurement of their diameters, transmission electron microscopy (TEM) was used for non-functionalized nanoparticles (MNP-OH, 8.91 nm), functionalized with initiator (NPN-I, 9.56), and for MNP-PHEMA-OH, MNP-PHEMA-FA1 and MNP-PHEMA-FA2 samples, transmission scanning electron microscopy (STEM) was used. STEM images (**figure II.10.d–f**) indicates an agglomeration trend for MNP-PHEMA-OH, MNP-PHEMA-FA1 and MNP-PHEMA-FA2 samples, accentuated by the drying process applied to the preparation of the TEM grids on which samples were deposited prior to STEM measurement.
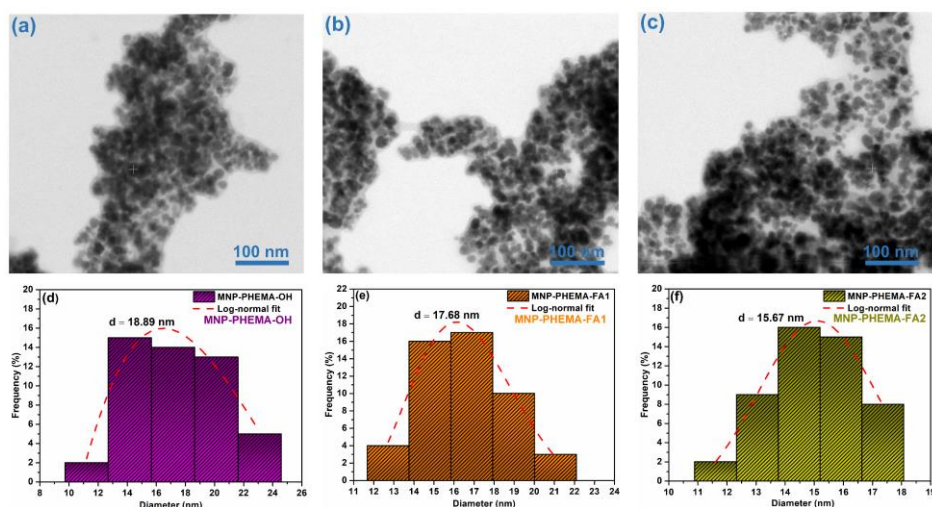
Figure II.10. STEM images and particle size distribution histograms of MNP-PHEMA-OH (a and d), MNP-PHEMA-FA1 (b and e), and MNP-PHEMA-FA2 (c and f) samples, respectively (Ghiarasim et al., 2021).

These nanoparticles were identified as core-shells (**figure II.10.a-c**) with average diameters of 18.89 nm (MNP-PHEMA-OH), 17.68 (MNP-PHEMA-FA1) and 15.67 nm (MNP-PHEMA-FA2) respectively (**figure II.10.d–f**). The observations obtained lead to two main conclusions regarding the morphology of the samples, firstly, the presence of folic acid in the structure of nanoparticles leads to an increase in their stability, and secondly, an increase in the FA concentration in the nanoparticle structure leads to a decrease in the size of core-shell nanoparticles.

Biologically the nanoparticles were biocompatible, both on the cell line NHDF and on three cancer cell lines (MCF-7, HeLa and HepG2). The cellular uptake of MNP-OH, MNP-PHEMA-OH and MNP-PHEMA-FA1 by NHDF, MCF-7, HeLa and HepG2 cell lines was determined by quantification of intracellular iron by thiocyanate method (Gupta and Gupta, 2005). In the case of interaction of nanoparticles with normal cells (NHDF), it was concluded that in this case the studied nanoparticles do not internalize into cells, whereas in the case of tumour cells a significantly higher internalisation is obtained compared to normal cells (**figure II.12.**).
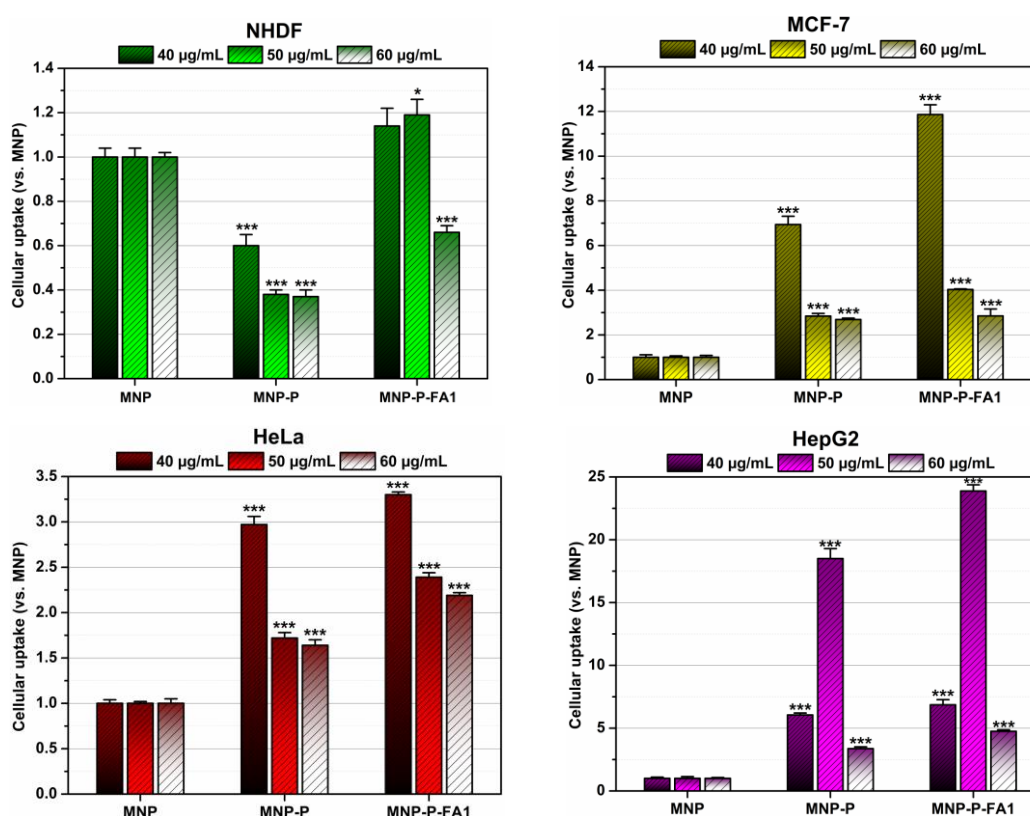
Figure II.12. Cellular uptake of MNP-OH, MNP-PHEMA-OH and MNP-PHEMA-FA1 nanoparticles (at concentrations of 40, 50 and 60 µg/mL) into normal NHDF cells and MCF-7, HeLa, HepG2 cancer cells after a 24-hour incubation. The experiments were conducted in triplicate. The iron content was determined by the thiocyanate method and the absorption of nanoparticles was reported to normalized MNP-OH nanoparticles. * $p < 0.05$, *** $p < 0.001$ against MNP-OH (for each concentration, the t-Student test was applied) (Ghiarasim et al., 2021).

Through atomic absorption spectrometry (the use of this method to determine intracellular iron content is much more sensitive compared to the thiocyanate method, and which can be used to detect very low iron concentrations), it has been confirmed that MNP-PHEMA-FA1/2 samples are better internalized into MCF-7 cells compared to NHDF cells (**figure II.13.**). In addition, the increase in FA content in the samples resulted in a slight increase in cellular uptake of MNP-PHEMA-FA2 compared to the MNP-PHEMA-FA1 sample.
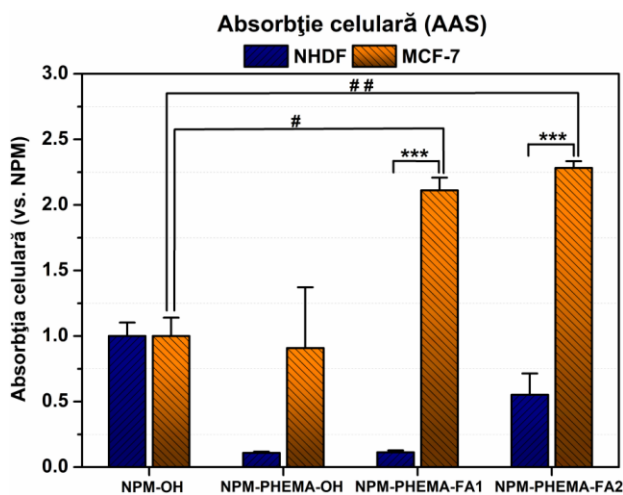
Figure II.13. Cellular uptake of samples MNP-OH, MNP-PHEMA-OH, MNP-PHEMA-FA1 and MNP-PHEMA-FA2 (40 µg/mL) in normal human dermal fibroblasts (NHDF) and mammary adenocarcinoma (MCF-7) after 24 for hours (Ghiarasim et al., 2021).

The MRI technique was used to evaluate the magnetic behaviour of nanoparticles used as a contrast agent. MNP-OH, MNP-PHEMA-OH, MNP-PHEMA-FA1 samples in PBS (pH = 7.4) at different concentrations were dispersed in 1% agar gel and were used for MRI relaxivity studies. In this analysis, relaxivities r1 and r2 were obtained, which led to the conclusion that an increase in Fe^{3+} concentration leads to a decrease in T2 value, and MRI images becomes darker (**figure II.15.**).
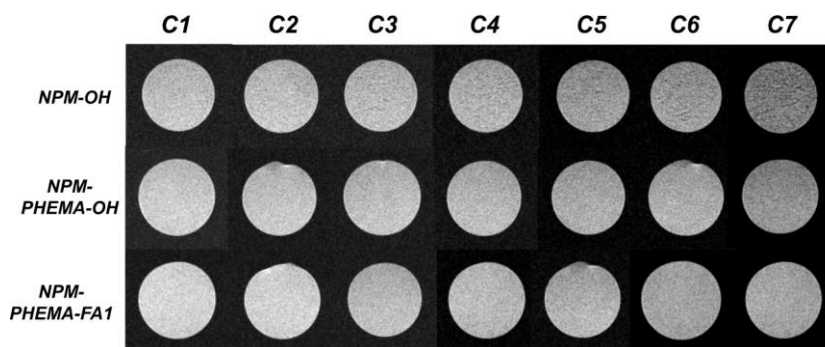
Figure II.15. T2-weighted MRI images of MNP-OH, MNP-PHEMA-OH and MNP-PHEMA-FA1 in the Fe3+ concentration range between 0,1 and 0,8 mM (C1-C7) showing negative contrast by increasing concentration (Ghiarasim et al., 2021).

It is worth mentioning that previous research in the literature has revealed that relaxivity is affected by the nature and thickness of the polymeric layer covering magnetic nanoparticles. In the present study, a slight decrease in the r2/r1 ratio is obtained in the MNP-PHEMA-FA1 sample compared to that of the MNP-PHEMA-OH sample, a decrease explained by the larger hydrodynamic diameter of the MNP-PHEMA-OH nanoparticles, which is consistent with previously published studies (Rowe et al., 2009; Najafian et al., 2015).

II.2.2. Magnetic nanoparticles decorated with three methacrylate polymers and functionalised with methotrexate

II.2.2.1. The motivation for the choice of methacrylate polymers and methotrexate

Methacrylate-type polymers are widely used in biomedical systems due to their biocompatibility and swelling ability, which allows for nonspecific interactions with cell membranes. The specific properties of these polymers have led them into various applications, including functionalization of magnetic nanoparticles, obtaining copolymer micelles, and

developing polymer-based hydrogels. These polymers have also been functionalized with biologically active molecules such as methotrexate and DNA oligonucleotides (Marikovsky, 1974; Marasini et al., 2022). Methotrexate (MTX) is a broad-spectrum drug used in the treatment of various conditions, starting with childhood leukemia in 1948 and becoming standard in the treatment of rheumatoid arthritis and breast cancer. Its complex mechanism of action involves inhibition of the enzyme dihydrofolate reductase, thereby disrupting DNA synthesis and cell proliferation. Due to this action, MTX has been integrated into various chemical systems for administration, such as magnetic nanoparticles decorated with polymers, liposomes, micelles, and prodrugs (Li et al., 2013; Nosrati et al., 2018; Guimarães et al., 2020; Carrillo-Castillo et al., 2020; Li et al., 2018).

II.2.2.2. Synthesis by SI-ATRP polymerization mechanism and physicochemical characterization of magnetic nanoparticles decorated with the three polymers +/- MTX

In this study, three methacrylate-type monomers (HEMA, PEGMA6 and PEGMA10) were polymerised by SI-ATRP, which were subsequently functionalised with methotrexate (**scheme II.2.**).
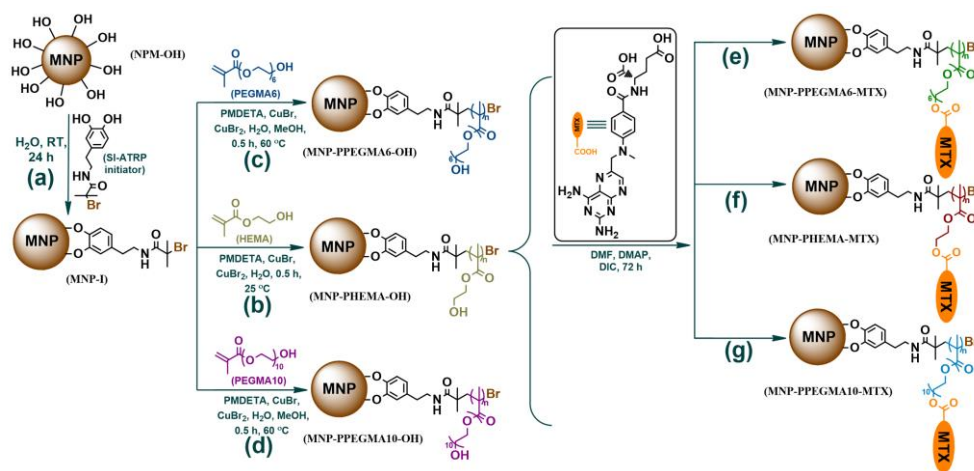
Scheme II.2. Synthesis steps to obtain three polymer-based nanoparticles functionalized with MTX.

A first technique used to monitor the synthesis steps in **scheme II.2.** was Fourier transform infrared spectroscopy (FTIR). Polymerisation of HEMA, PEGMA6 and PEGMA10 monomers by SI-ATRP (**figure II.16.a.**) was highlighted by the disappearance of bands from the spectra of polymer-decorated nanoparticles, of the C=C vibration band specific to monomers.
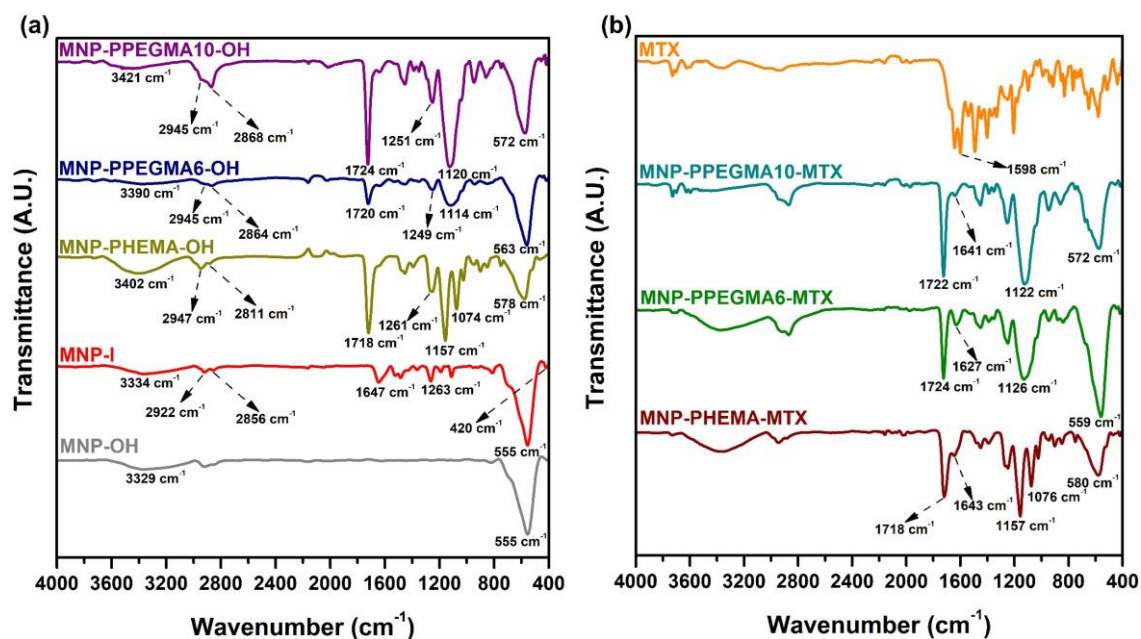
Figure II.16. (a) FTIR spectra of non-functionalized magnetic nanoparticles (MNP-OH), with ATRP-type initiator (MNP-I) and the three polymers obtained by SI-ATRP (MNP-PHEMA-OH, MNP-PPEGMA6-OH and MNP-PPEGMA10-OH), (b) FTIR spectra of magnetic nanoparticles decorated with the three MTX-functionalized polymers (MNP-PHEMA-MTX, MNP-PPEGMA6-MTX and MNP-PPEGMA10-MTX, respectively) and free MTX.

The functionalization of polymers grown on the surface of magnetic nanoparticles with MTX led to the appearance of vibrational bands for amide bond stretching (**figure II.16.b.**) at 1598 cm^{-1}, 1643 cm^{-1}, 1627 cm^{-1}, 1641 cm^{-1} in the FTIR spectra corresponding to MTX, MNP-PHEMA-MTX, MNP-PPEGMA6-OH and MNP-PPEGMA10-MTX samples respectively.

UV-Vis spectroscopy was used to quantify the concentration of MTX covalently bound to hydroxyl groups on each type of polymer structural unit (calibration curve method was used). Thus, the determined concentrations of MTX in nanoparticles were 61.4 μg MTX / mg MNP-PHEMA-MTX, 131 μg MTX / mg MNP-PPEGMA6-MTX and 58.4 μg MTX / mg MNP-PPEGMA10-MTX. These values represent the amount of MTX per milligram of the corresponding functionalized magnetic nanoparticles.

For the physicochemical analysis of these nanoparticles, other characterization techniques were used, such as thermogravimetric analysis, calorimetry with differential scanning, superparamagnetic behaviour was determined by measuring magnetic properties.

Each change in the surface of the synthesized magnetic nanoparticles influences the hydrodynamic diameter of the nanoparticles. Thus, using the DLS technique, the average hydrodynamic diameters of all samples involving magnetic nanoparticles from **scheme II.1** (**figure II.23.a.** and **II.23.b.**).
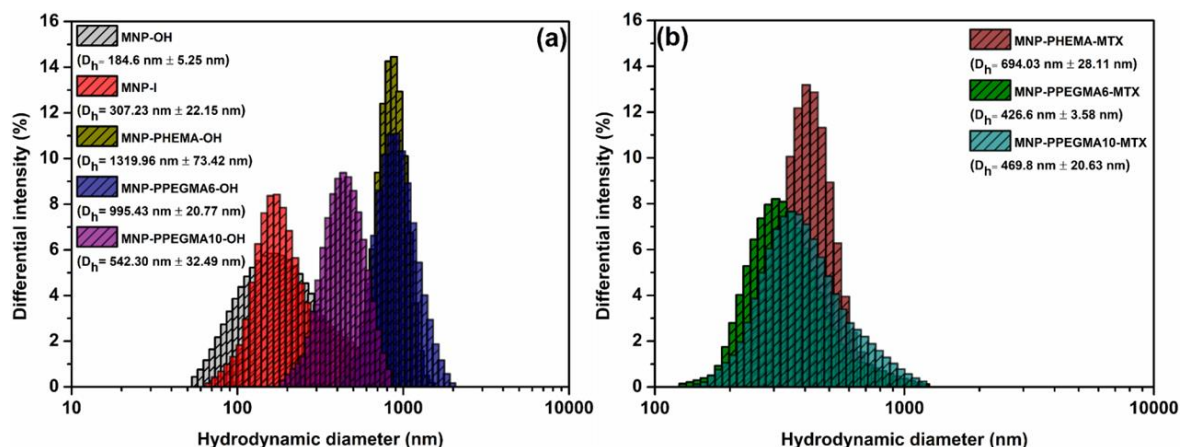
Figure II.23. (a) Average hydrodynamic diameters of magnetic nanoparticles MNP-OH, MNP-I, MNP -PHEMA-OH, MNP-PPEGMA6-OH and MNP-PPEGMA10-OH and (b) MNP-PHEMA-MTX, MNP-PPEGMA6-MTX and MNP-PPEGMA10-MTX, dispersed in PBS at pH = 7,4.

The polymerisation of monomers has led to an increase in hydrodynamic diameters of nanoparticles (**figure II.23.a.**) and subsequently their functionalisation with MTX at a decrease, behaviour observed for all three monomers (**figure II.23.b.**).

To highlight the morphology and size of nanoparticles, both unmodified and modified, scanning transmission electron microscopy (STEM) was used. In **figure II.25.**, can be observed in the case of unmodified magnetic nanoparticles (MNP-OH, **figures II.25.a.** and **II.25.c.**) and those with an ATRP-type initiator grafted onto the surface of nanoparticles (MNP-I, **figures II.25.b.** and **II.25.d.**), an agglomeration trend, showing spherical shapes, with an average diameter of 10.36 nm ± 2.01 nm for the MNP-OH sample and 13.16 nm ±1.75 nm for the MNP-I sample, respectively. After polymerization of the three monomers by SI-ATRP, the nanoparticles are presented as a core-shell with average diameters larger than the diameters of the previous samples (MNP-OH and MNP-I), where the "core" is given by the magnetic nanoparticles and the "shell" given by the polymer shell. These structures take the form of aggregates obtained after evaporation of the solvent. Thus, the MNP-PHEMA-OH sample (**figure II.26.a.** and **II.26.d.**) had an average diameter of 19.41 nm ±

Figure II.25. STEM images and distribution histograms of unmodified magnetic nanoparticle (MNP-OH) diameters (a) and (c) and those decorated with ATRP initiator (MNP-I), (b) and (d).

5.05 nm followed by an average diameter of 19.17 nm ± 3.19 nm in the case of MNP-PPEGMA6-OH and (**figure II.26.b.** and **II.26.e.**) and an average diameter of 22.99 nm respectively ± 4.53 nm for MNP-PPEGMA10-OH sample (**figure II.26.c.** and **II.26.f.**), clearly indicating that the size of the nanoparticle is influenced by the length of the macromolecular chain attached to the surface of the same inorganic nanoparticle.
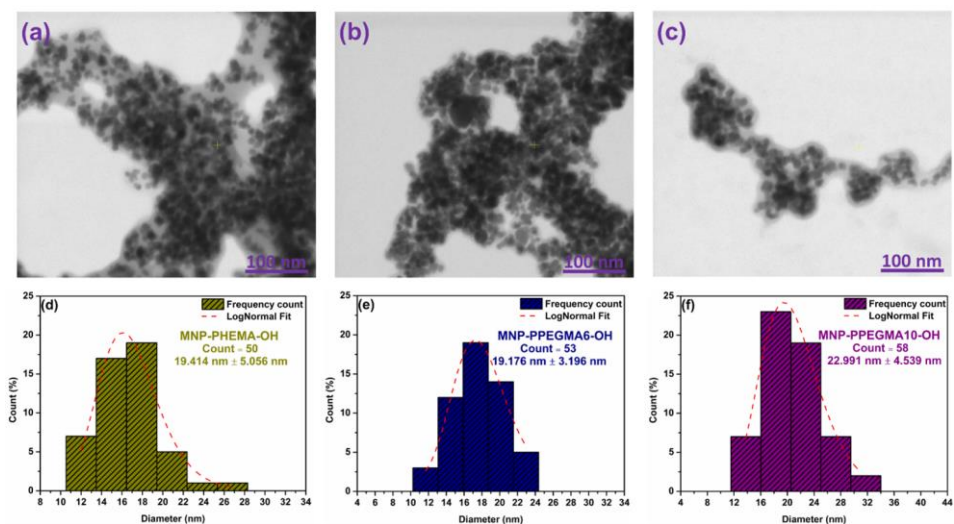
Figure II.26. STEM images and histograms of nanoparticle diameter distribution: MNP-PHEMA-OH (a) and (d), MNP-PPEGMA6-OH (b) and (e) and MNP-PPEGMA10-OH (c) and (f).

The functionalization of polymers with MTX led to a decrease in average diameters compared to polymer nanoparticles, due to the reduction of the "non-fouling" property of polymers, leading to obtaining nanoparticles with smaller average diameters, which is also supported by the results obtained by DLS (Ghiarasim et al., 2021).
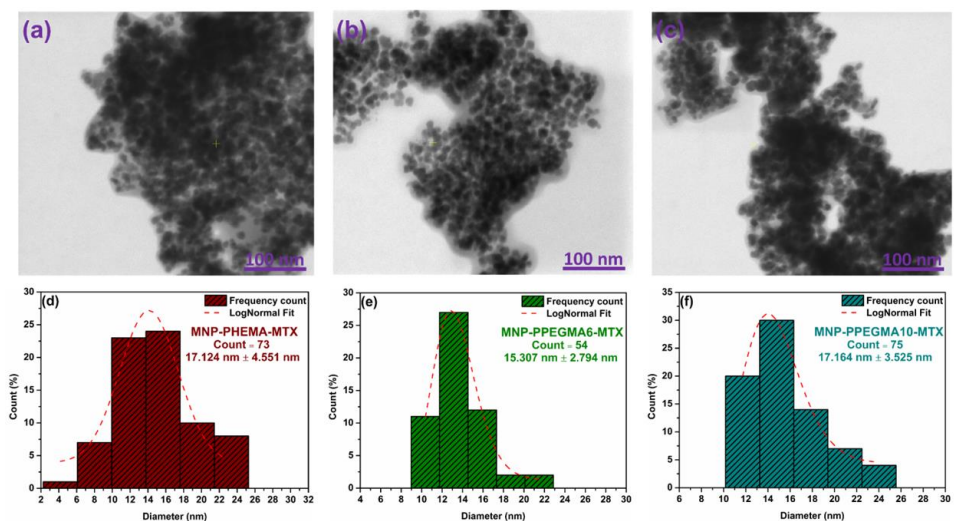
Figure II.27. STEM images and histograms of magnetic nanoparticle diameter distribution decorated with the three MTX-functionalized polymers (MNP-PHEMA-MTX (a) and (d), MNP-PPEGMA6-MTX (b) and (e) and MNP-PPEGMA10-MTX (c) and (f).

Thus, the MNP-PHEMA-MTX sample (**figures II.27.a.** and **II.27.d.**) had an average diameter of 17.12 nm ± 4.55 nm followed by an average diameter of 15.30 nm ± 2.79 nm measured for MNP-PPEGMA6-MTX sample (**figures II.27.b.** and **II.27.e.**) and 17.16 nm

respectively ± 3.52 nm assigned to MNP-PPEGMA10-MTX sample (**figures II.27.c.** and **II.27.f.**).

To determine the biocompatibility of starting and functionalized nanoparticles with MTX, the CellTiter-Glo® test on human gingival fibroblasts (HGF) and their cytotoxicity on breast adenocarcinoma cells (MCF-7) after an incubation time of 72 hours was used. The results concluded that magnetic nanoparticles with the three decorated polymers on their surface (MNP-PHEMA-OH, MNP-PPEGMA6-OH and MNP-PPEGMA10-OH) were biocompatible, not affecting the viability of HGF cells at the concentrations tested. MTX polymer functionalization did not significantly alter the viability of normal fibroblasts but had a pronounced effect on MCF-7 cells, reducing their viability by up to 69% (**figure II.29**).
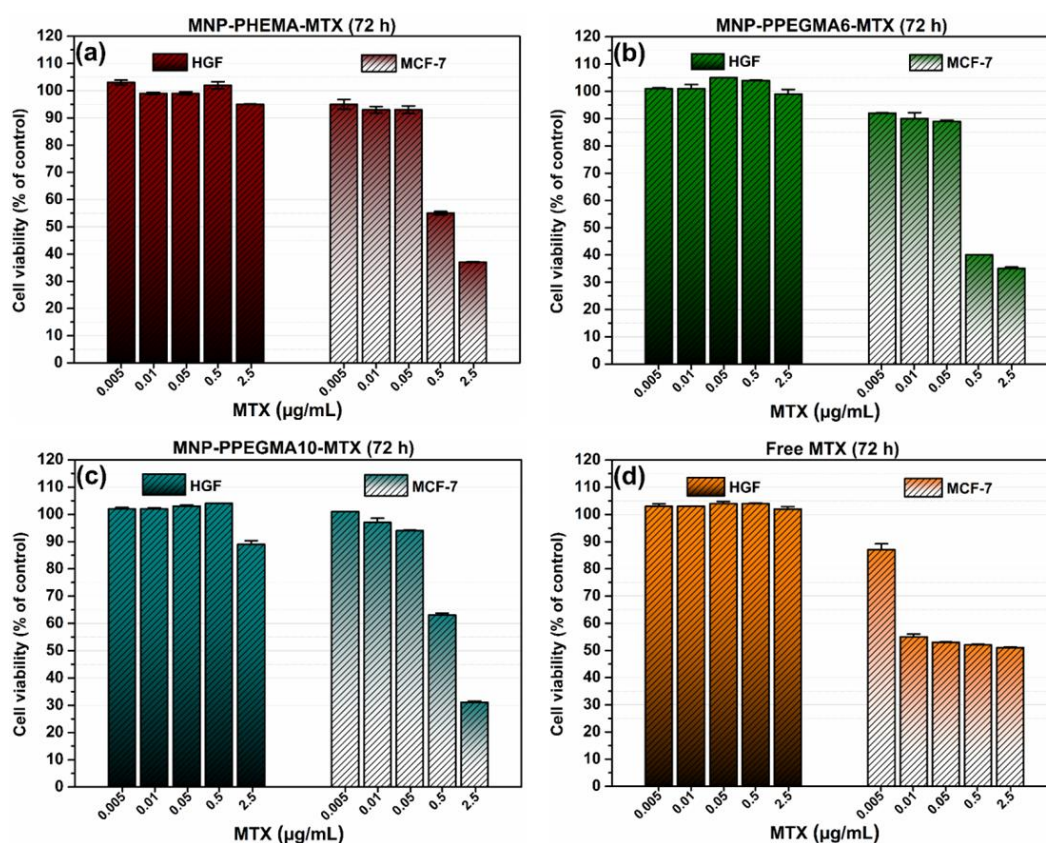
Figure II.29. Cytotoxicity of magnetic nanoparticles decorated with the three polymers functionalized with MTX (MNP-PHEMA-MTX (a), MNP-PPEGMA6-MTX (b), MNP-PPEGMA10-MTX (c) and free MTX (d), respectively, at different concentrations on HGF and MCF-7 cell lines.

Methotrexate in the native state did not alter the viability of normal fibroblasts at concentrations up to 2.5 μg/mL, but induced cell death up to 49% in MCF-7 cells at the same concentration. MTX-functionalized nanoparticles induced cytotoxicity in MCF-7 cells at concentrations higher than 0.05 μg/mL, in contrast to free MTX which induced a plateau of approximately 55% cell viability.

CHAPTER III – Micelles based on biocompatible polymers for the development of new approaches in the effective treatment of breast cancer

III.1. Motivation and objectives of the study related to Chapter III

III.1.1. Specific scientific objectives:

I. Design, obtaining and physicochemical characterization of poly(ethylene glycol)-co-polyhistidine (PEG-PHis) diblock copolymers with length-controlled PHis sequence for the preparation of functional self-assembled nanostructures.

II. Study of the self-assembly process of PEG-PHis copolymers in uniform micelles with controlled dimensions, loading micelles with an antitumor drug and establishing the optimal length of the polyhistidine chain for the release of the active principle at pH values specific to tumour tissues.

III. *In vitro* testing of drug-loaded copolymers and micelles on breast cancer-specific cell lines (MDA-MB-231).

IV. Functionalization of the surface of micelles with a monoclonal antibody (trastuzumab) specific to breast cancer and *in vitro* evaluation of biological activity of micelles decorated with trastuzumab on 2D and 3D cell cultures, respectively.

III.1.2. Motivation for the use of polyethylene glycol-polyhistidine diblock copolymers

In recent decades, interest in pH-sensitive materials, which remain stable at physiological pH and break down at lower pH found in tumour environments, has increased significantly. These materials, drug-loaded or functionalised with various molecules, are essential for the development of nanosystems used in targeted drug transport and delivery, especially in cancer treatment. pH-sensitive chemical systems such as core-shell micelles and peptide-polymer copolymers offer promising solutions for this purpose. The synthesis of these materials may involve the incorporation of carboxylic groups, the covalent binding of drug molecules, or the use of pH-sensitive organic fragments, which cause structures to disassemble at specific pH. However, the complexity of the synthesis of diblock copolymers may represent a limitation in the application of these systems. The synthesis of peptides on solid support (SPPS) offers an affordable and efficient alternative for obtaining copolymers, opening new perspectives for the development of intelligent drug delivery systems (Samaritoni et al., 2018).

III.2. Results and discussion

III.2.1. Design, synthesis and assembly of PEG-PHis copolymers in micelles in the absence or presence of an antitumour drug

In this study, three PEG-PHis-based copolymers were designed to be synthesized using the SPPS technique. The structure of the copolymers proposed for synthesis included a 2 kDa molecular weight PEG unit, to be covalently bonded to a polyhistidine chain with a chain length of 20, 26 and 32 structural amino acid units (L-histidine). Also, polyhistidine sequences were thought to include a lysine unit at the end of the chain to allow covalent binding of fluorophores with free amine in the lysine structure. At the other end of the polyhistidine chain, a cysteine unit was added, allowing the attachment of the PEG chain by a specific reaction between the thiol group of cysteine and the maleimide group attached to the end of the PEG chain (chemical structures of copolymers are represented in **figure III.1.** (Nanda and Lorsch, 2014).
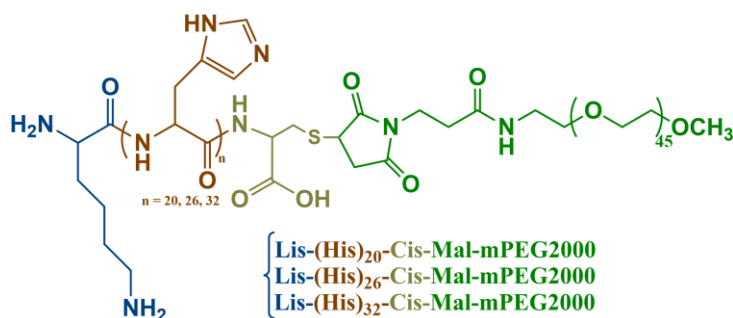
Figure III.1. The general chemical structure of the three copolymers synthesized by the SPPS technique (blue - lysine, red - histidine, yellow - cysteine, and green - PEG, respectively).

The engineered copolymers were synthesized in collaboration with Chempeptide Ltd. (Shanghai, China) using SPPS technique. They were analysed using mass spectrometry (MS) and high-performance liquid chromatography (HPLC). Subsequently, the three copolymers were assembled in micelles in the absence/presence of an antitumor drug called doxorubicin (DOX) used as a model compound (Ghiarasim et al., 2022). The stages of obtaining unloaded and DOX-loaded micelles are represented in **scheme III.1.**
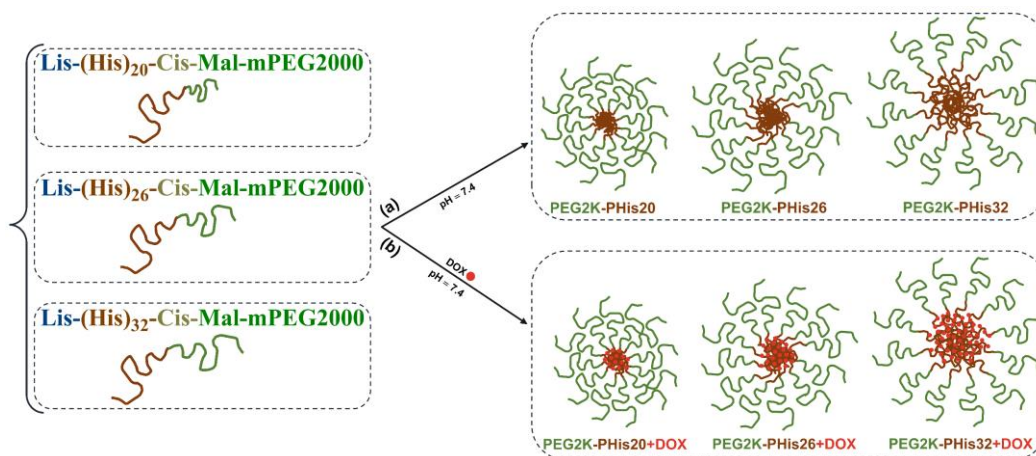
Scheme III.1. Assembly of the three copolymers into unloaded micelles (a) and DOX-loaded micelles (b), respectively.

A first parameter calculated for these micelles was the critical micelle concentration (CMC) for each copolymer (0.111 mg/mL for mPEG-2000-Mal-Cis-(His)20-Lis, 0.045 mg/mL for mPEG-2000-Mal-Cis-(His)26-Lis and 0.032 mg/mL for mPEG-2000-Mal-Cis-(His)32-Lis copolymer). This parameter was calculated using a standardized method involving pyrene as a fluorescent compound and fluorescence spectroscopy. The decrease in CMC values from 0.111 mg / mL to 0.032 mg / mL with increasing polyhistidine chain length was because the hydrophobicity of the system that contributed to the formation of micelles at lower copolymer concentrations at pH = 7.4 also increased, and the CMC values obtained for PEG2K-PHis20/26/32 copolymers agreed with the values obtained in previous studies (Lee et al., 2003).

The hydrodynamic diameters obtained by the DLS technique conclude that an increase in the length of the PHis chain in the structure of the copolymers leads to an increase in hydrodynamic diameters, both for unloaded and DOX-loaded ones. To highlight the morphology of formed micelles, both unloaded and DOX-loaded, scanning transmission electron microscopy (STEM) was used. In **figure III.7.** STEM images of PEG2K-PHis20/26/32 micelles are presented, highlighting their assembly into nanometric spherical formations. In the case of sample PEG2K-PHis20 (**figure III.7.a.**), a core-shell structure with an average diameter of 232 nm ± 33 nm (**figure III.7.d.**), with a strong contrast of the hydrophobic part ("core") due to polyhistidine chains, which have a higher electron density compared to the hydrophilic PEG shell. The PEG2K-PHis26 sample showed an average diameter of 112 nm ± 26 nm (**figure III.7.e.**), while the PEG2K-PHis32 sample had an average diameter of 89 nm ± 20 nm (**figure III.7.f.**).
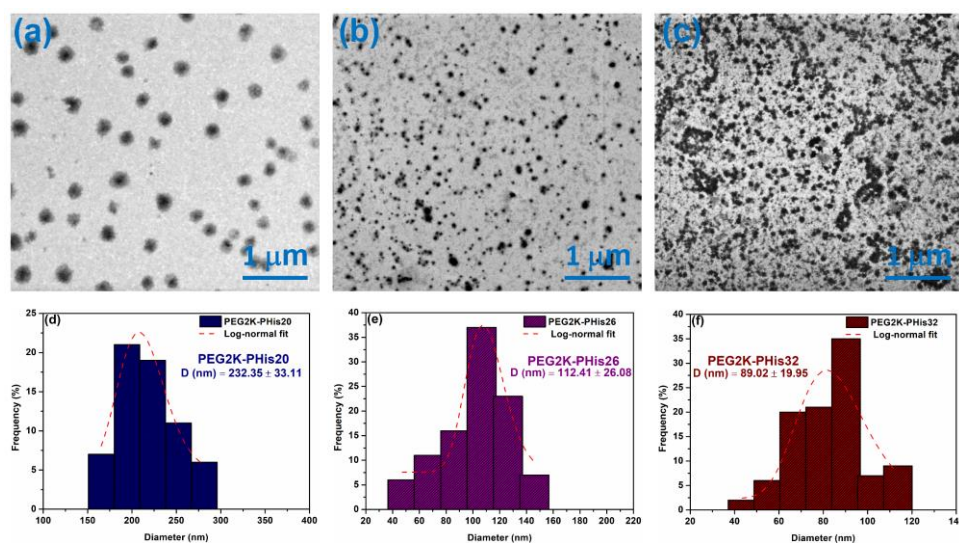
Figure III.7. Scan transmission electron microscopy (STEM) images of unloaded micelles (a – c) and diameter distribution (d – f) (Ghiarasim et al., 2022).

Analysing the diameters of unloaded micelles, it was observed that the average diameter decreased with increasing polyhistidine chain length, results that contradict DLS data. This may be due to the greater stability of micelles with longer polyhistidine chains, due to stronger

interactions involved in micelle formation. The more compact assembly of longer polyhistidine chains was also reflected in obtaining a more intense contrast of the inner part of the micelles, a contrast observed in STEM images from **figures III.7.b to c** for PEG2K-PHis26 (b) and PEG2K-PHis32 (c) samples.

In the case of DOX-loaded micelles, STEM images also showed uniform spherical assemblies with much higher contrast due to the micelles' loading with DOX molecules (**figure III.8.**).
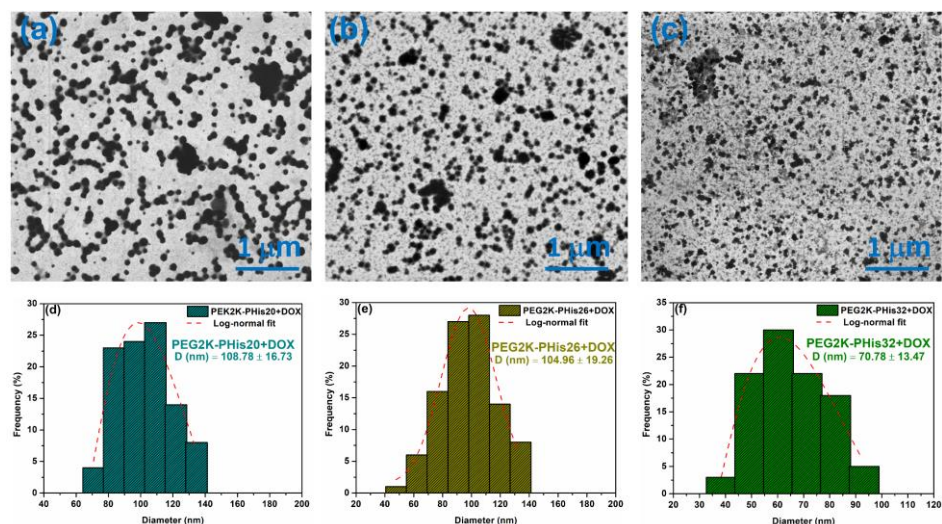
Figure III.8. STEM images of DOX-loaded micelles (a-c) and diameter distribution (d-f) (Ghiarasim et al., 2022).

Analysing in detail **figure III.8.a - c**, it can be noted that all samples in the STEM images revealed a gradual decrease in mean diameters compared to unloaded micelles (**figure III.8.d - f**), PEG2K-PHis20+ DOX with a mean diameter of 109 nm ± 17 nm, PEG2K-PHis26+DOX with 105 nm ± 19 nm and PEG2K-PHis32+DOX with a mean diameter of 71 nm ± 13 nm), indicating strong nonspecific hydrophobic interactions of polyhistidine chains with DOX molecules. In addition, DOX can form compact nanocrystals inside micelles, where this phenomenon has been observed in similar chemical systems, leading to better compaction of the micelles' core (Cipolla et al., 2016). Compaction of micelles with DOX molecules also generated unexpected stabilization in all three samples studied (in according with **figure III.8**).

The concentration of loaded DOX in micelles was determined by fluorescence spectroscopy (**figure III.9.**), using a calibration curve (free DOX) as a function of fluorescence intensity at 592 nm vs wavelength. Unloaded micelles showed no fluorescence emission, while DOX-loaded micelles showed DOX-corresponding emissions, with intensities strongly dependent on the concentration of drug loaded into micelles. From the studies performed, the following values of DOX concentrations loaded in one mg of each studied copolymer were obtained: 73.8 μg DOX for PEG2K-PHis20+DOX micelles, 128.4 μg DOX for PEG2K-PHis26+DOX and 181.2 μg for PEG2K-PHis32+DOX micelles, respectively. The

concentration of DOX in micelles gradually increased with increasing length of the PHis chain in the structure of copolymers. This increase is correlated with STEM data on the higher degree of compaction of DOX molecules loaded into micelles.
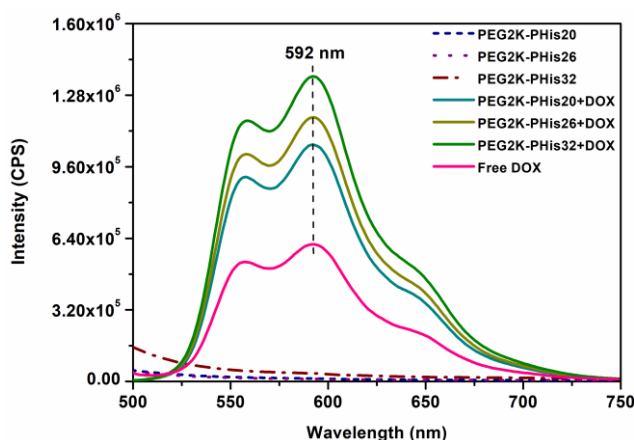
Figure III.10. Overlap of emission spectra of native DOX and unloaded and DOX-loaded micelles, with highlighting the maximum emission of DOX from 592 nm, $\lambda_{excitation} = 480$ nm (Ghiarasim et al., 2022).

Table III.2. Efficiency of encapsulation (EE) and drug loading (DL) of DOX into PEG2K-PHis20+DOX, PEG2K-PHis26+DOX and PEG2K-PHis32+DOX micelles (Ghiarasim et al., 2022).

Sample	EE (%)	DL (%)
PEG2K-PHis20+DOX	52.98	8.11
PEG2K-PHis26+DOX	60.51	9.16
PEG2K-PHis32+DOX	71.31	10.62

Within this subchapter of the doctoral thesis, a DOX release study was performed from the micelles PEG2K-PHis20+DOX, PEG2K-PHis26+DOX, PEG2K-PHis32+DOX at a temperature of ℃, by changing the pH of the medium, in the range of 6.5 and 6.9 to simulate the extracellular environment of cancer cells (Chen et al., 2017) (dialysis method). The pH values investigated in this study were 7.4 (the value at which DOX-loaded micelles were assembled), 7.2 and 6.5 (specific to the tumor extracellular environment) in PBS aqueous solution with appropriate pH adjustment. It is important to note that the value of pH = 7.0 was excluded from the experiment because at this pH value, DOX forms dimers that favor its precipitation from solution (Yamada, 2020) and thus lead to the impossibility of quantifying the concentration of the drug. In addition, the release time of the study was limited to 10 hours to avoid prolonged exposure of DOX in an aqueous solution, which can also lead to precipitate formation and erroneous results.
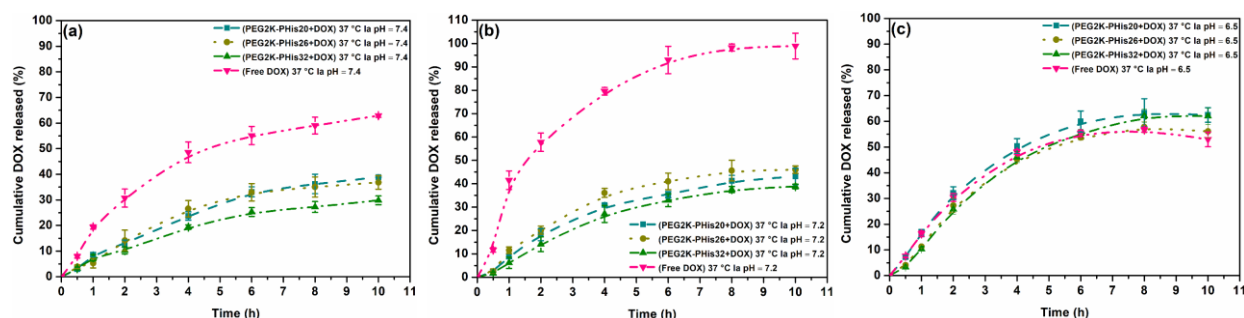
Figure III.11. DOX release curves from DOX-loaded micelles (PEG2K-PHis20+DOX, PEG2K-PHis26+DOX, PEG2K-PHis32+DOX) and free DOX in PBS solution at pH = 7,4 (a), pH = 7,2 (b) and pH = 6,5 (c) at 37 ℃ (Ghiarasim et al., 2022).

Analysing release curves in **figure III.11.**, after 10 hours, the percentage of cumulative DOX release from PEG2K-PHis32+DOX micelles was approximately 20 - 24% at pH = 7.4, with a slight increase in the percentage of release at pH of 7.2. This difference in release percentages led to the conclusion that the micelles in this DOX-loaded study are sensitive to small variations in pH towards acidic pH, on the one hand, and on the other hand, once the length of the PHis chain increased, the micelles became more stable at physiological pH of 7.4. At pH = 6.5, the cumulative DOX release from PEG2K-PHis20+DOX and PEG2K-PHis26+DOX samples was equivalent to that of PEG2K-PHis32+DOX but was at least twice as high as at pH = 7.2 and pH = 7.4, where a 6-hour release plateau was observed for all samples. When the pH dropped to 6.5, the PHis in all samples was fully protonated, therefore the percentage of drug release increased significantly compared to the percentages obtained at pH = 7.2 (**figure III.11.c.**). This last aspect is of particular interest because, at pH = 6.5, which is the lower limit of extracellular pH in the case of cancer cells, the micelles released over 50% DOX, thus demonstrating the potential of the micelles studied as effective for chemical systems with the property of releasing drugs into extracellular tumour environment (Chen et al., 2017).

To further evaluate the stability, cytotoxicity, and release properties of both unloaded and DOX-loaded micelles, an evaluation was performed *in vitro* studies on human triple-negative cells (MDA-MB-231) over a period of 72 hours (**figure III.14**), and these results indicated controlled release of DOX from micelles.
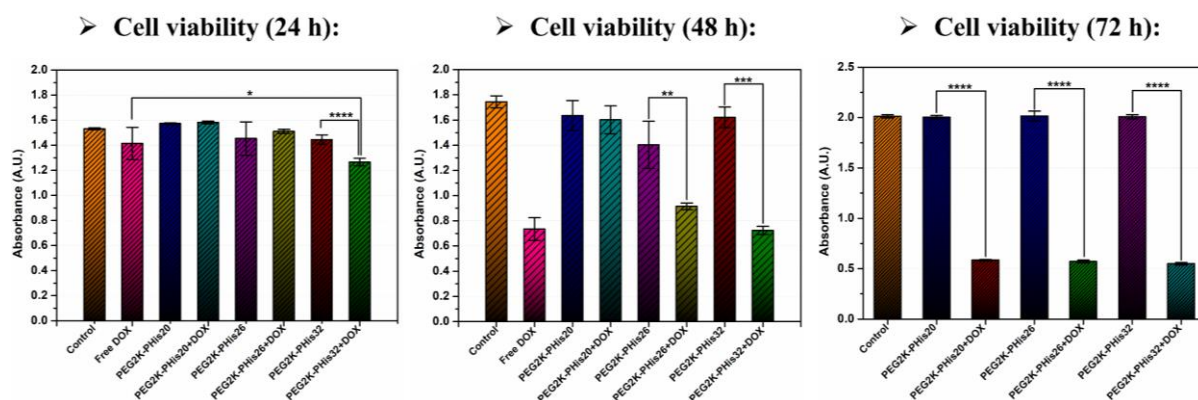
Figure III.14. Effects of DOX unloaded micelles, and DOX-loaded micelles on MDA-MB-231 breast cancer cells. Cell viability was determined at 24, 48 and 72 hours, expressed as absorbance. *p<0.05, **p<0.005, ***p<0.0005, ****p<0.00005.

III.2.2. Functionalization of PEG-PHis micelles with trastuzumab

III.2.2.1. Motivation for use of trastuzumab monoclonal antibody

The standard treatment for HER2-positive breast cancer is to administer the anti-HER2 monoclonal antibody called trastuzumab (Tzm, with the trade name Herceptin). This treatment was effective for both early and advanced stages of breast cancer due to trastuzumab binding

to the p185 HER2 glycoprotein transmembrane receptor and causing apoptosis of tumor cells or preventing their growth. Although a significant number of patients with HER2+ breast cancer benefit from anti-HER2 therapy, a subset of patients develop resistance, which ultimately leads to disease advancement (Adam-Artigues et al., 2022; Valabrega, Montemurro and Aglietta, 2007; Nahta et al., 2006).

It has previously been found that binding of Tzm to different types of nanoparticles does not affect its ability to bind specifically to overexpressed HER2 transmembrane receptors in breast cancer-specific tumor cells. This is further reinforced by the emergence of U.S. Food and Drug Administration (FDA)-approved Tzm-based chemical conjugates of chimeric monoclonal antibody type such as margetuximab (Gradishar et al., 2023) and antibody-drug type systems such as trastuzumab-DM1 (von Minckwitz et al., 2019) or trastuzumab deruxtecan (Modi et al., 2022). In the present study, the PHis-PEG diblock copolymer was used to obtain micelles that were subsequently functionalized on the surface with Tzm in a controllable way, obtaining a functionalized nano-assembled system, leading to exceptional and unexpected results on HER2+ cells on 2D and 3D cell cultures.

III.2.2.2. Obtaining and physicochemical characterization of trastuzumab functionalized micelles

The diblock copolymer (H_2N-PEG-2000-Mal-Cis-(His)32) synthesized by SPPS consists of a polymer chain of PEG (2kDa) and a polymer chain of PHis with 32 repetitive monomer units of L-histidine. The PEG sequence used in SPPS synthesis contains a free terminal amine group, which plays a role in the covalent binding of Tzm to the surface of the micelles obtained (**scheme III.2.**). Copolymer H_2N-PEG-2000-Mal-Cis-(His)32 was reacted with the sodium salt of 3-sulfo-N-succinimimidyl 4-(N-maleimidomethyl)cyclohexane-1-carboxylate (sulfo-SMCC, maleimide-type linker) in PBS solution in a molar ratio of 1:5 to introduce a terminal maleimide group onto the end of the PEG in the copolymer structure. The excess of unreacted sulfo-SMCC molecules was removed by repeated washings to obtain the maleimide-functionalised copolymer (Linker-PEG-2000-Mal-Cis-(His)32), suitable for reaction with Tzm. Later this copolymer was assembled into micelles (Linker-PEG2K-PHis32) around physiological pH (pH = 7.6), due to the hydrophobicity of the PHis polymer and the hydrophilicity of the PEG polymer (Hu et al., 2013; Kim, Bae and Jo, 2005; Lee et al., 2003b).
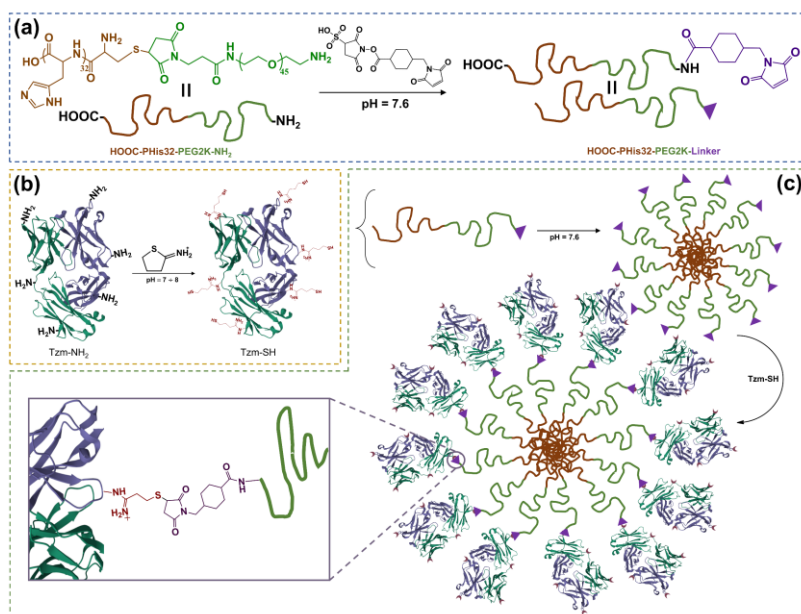
Scheme III.2. Stages of assembly of copolymers in micelles functionalized with monoclonal antibody: a) covalent binding of a maleimide derivative to the terminal amine group in the structure of the PEG, b) transformation of free amino groups from unchanged Tzm (Tzm-NH2) into thiol groups (Tzm-SH) using Traut reagent and c) self-assembly of functionalized copolymer molecules with malemide-type linker into well-defined micelles, followed by covalent attachment of Tzm-SH to the surface of micelles.

To functionalize Linker-PEG2K-PHis32 micelles with trastuzumab, Tzm-NH$_2$ (commercial trastuzumab) was reacted with Traut's reagent (2-iminothiolane hydrochloride) to produce the corresponding Tzm-SH, according to the protocol previously reported in the literature (Kulhari et al., 2016). The quantification of the number of thiol groups obtained on each molecule of Tzm-SH was performed by the Ellman test (Ellman, 1959), using UV-Vis spectroscopy (**figure III.16.**), resulting in 3,36 thiol groups per molecule of Tzm-SH.
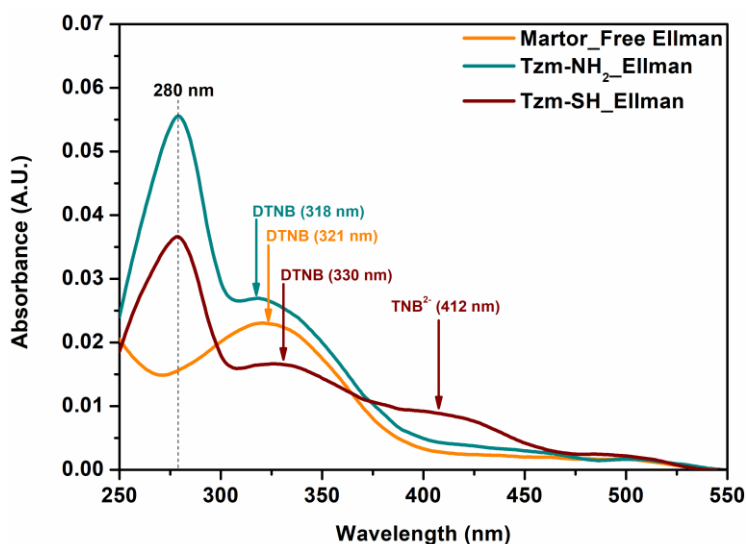
Figure III.16. UV-Vis absorption spectra of Ellman's reagent (free Martor_Ellman), unchanged trastuzumab after reaction with Ellman's reagent (Tzm-NH2_Ellman) and modified trastuzumab after reaction with Ellman's reagent (Tzm-SH_Ellman), respectively.

Size variations and changes in the surface of micelles were monitored by measuring hydrodynamic diameters (**figure III.17.**) and the successful covalent binding of Tzm to the surface of micelles was evidenced by changing the value of the zeta potential of micelles (**table III.4.**).

31

Table III.4. Mean values of zeta potentials (ζ) measured by dynamic light diffusion (DLS) technique for PEG2K-PHis32, Linker-PEG2K-PHis32 and Tzm-PEG2K-PHis32 micelles, respectively, dispersed in PBS at pH = 7.6.

Sample	ζ (mV) ± SD
PEG2K-PHis32	7.96 ± 0.17
Linker-PEG2K-PHis32	− 3,82 ± 0,78
Tzm-PEG2K-PHis32	− 5,53 ± 0,53
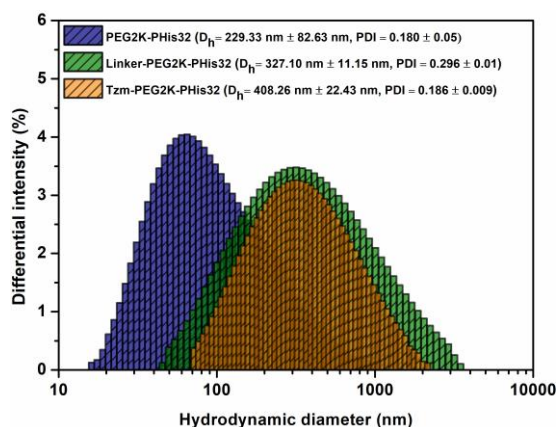
Figure III.17. Hydrodynamic diameters (Dh) and mean polydispersity indices (PDI) of PEG2K-PHis32, Linker-PEG2K-PHis32, Tzm-PEG2K-PHis32 micelles measured by dynamic light diffusion (DLS) technique, dispersed in PBS at pH = 7.6.

Morphologically, micelles were further analysed using scanning transmission electron microscopy (STEM) (**figure III.18.**). The diameters measured using this technique were significantly smaller compared to hydrodynamic diameters determined by DLS ((a) PEG2K-PHis micelles with a diameter of 59.49 nm ± 9.71 nm, (b) Linker-PEG2K-PHis32 with 78.56 nm ± 7.42 nm, and (c) Tzm-PEG2K-PHis32 micelles showing a diameter of 104.05 nm ± 11.98 nm). This reduction in size can be attributed to dehydration of micelles that occurs during the process of preparing samples for STEM analysis (Peng et al., 2019).
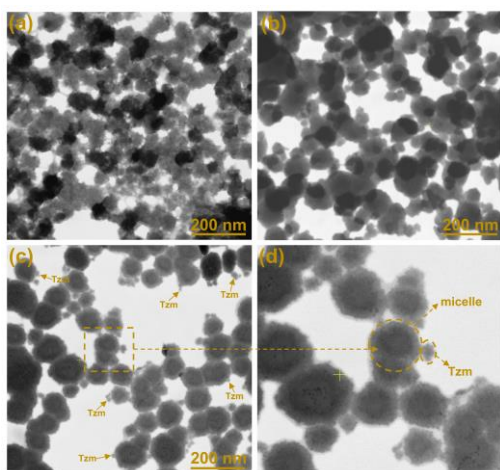
Figure III.18. STEM images of PEG2K-PHis32 (a), Linker-PEG2K-PHis32 (b), Tzm-PEG2K-PHis32 (c) micelles with magnification of the area in image (c) where the attachment of Tzm to the surface of micelles (d) is highlighted.
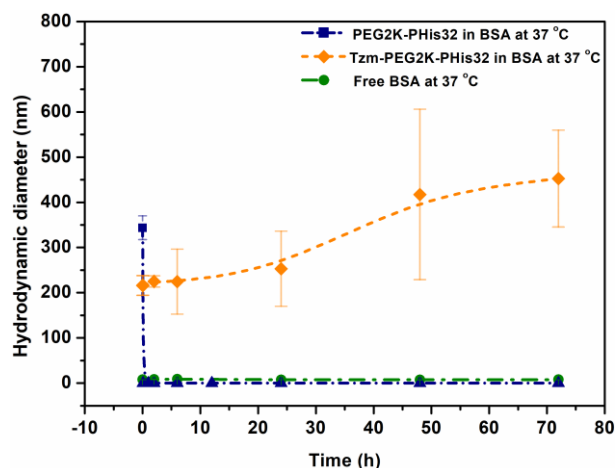
Figure III.20. Variations in mean hydrodynamic diameters for PEG2K-PHis32, Tzm-PEG2K-PHis32 micelles and free BSA measured by DLS in presence of BSA (70 mg/mL) at 37 ℃ over a 72-hour period.

The stability of the micelles in the presence of bovine serum albumin (BSA) was established by monitoring the variations in hydrodynamic diameters following their interaction with BSA molecules (Leeman et al., 2018). The stability study was conducted at a temperature of 37 ℃ (**figure III.20.**) over 72 hours, using a micelles concentration above the critical micelle

concentration (CMC) obtained in the first study of this thesis chapter. The micelles that were not functionalized after 5 minutes of interaction with BSA molecules were completely destabilized. In the case of micelles Tzm-PEG2K-PHis32 (**figure III.20.**), following interaction with BSA molecules, they exhibited different behaviours than the previous sample. After 5 minutes of interaction with the BSA, the mean hydrodynamic diameter of the micelles increased over the 72-hour period. This increase has been attributed to the pronounced affinity of BSA molecules to form aggregates at the surface of micelles (Peng et al., 2019).

Micelles (non-functionalized and functionalized) were biocompatible on cells HGF, viability tested at 72 hours. To highlight the effectiveness of micelles functionalized with Tzm, three types of PEG2K-PHis32 micelles with different concentrations of Tzm (2, 4 and 8 µg Tzm/mL of micelles) were prepared. These micelles, as well as free Tzm (free trastuzumab, Tzm-NH$_2$) at the three concentrations used for functionalization, were tested on three breast cancer-specific cell lines expressing the HER2 receptor on the cell surface in 2D cell cultures: SK-BR-3 (Tzm-response cell line), BT-474 (also showing Tzm response) and MDA-MB-361 (with an intermediate Tzm response) (**figure III.23.**).

➤ **SK-BR-3 cell line:** ➤ **BT-474 cell line:** ➤ **MDA-MB-361 cell line:**
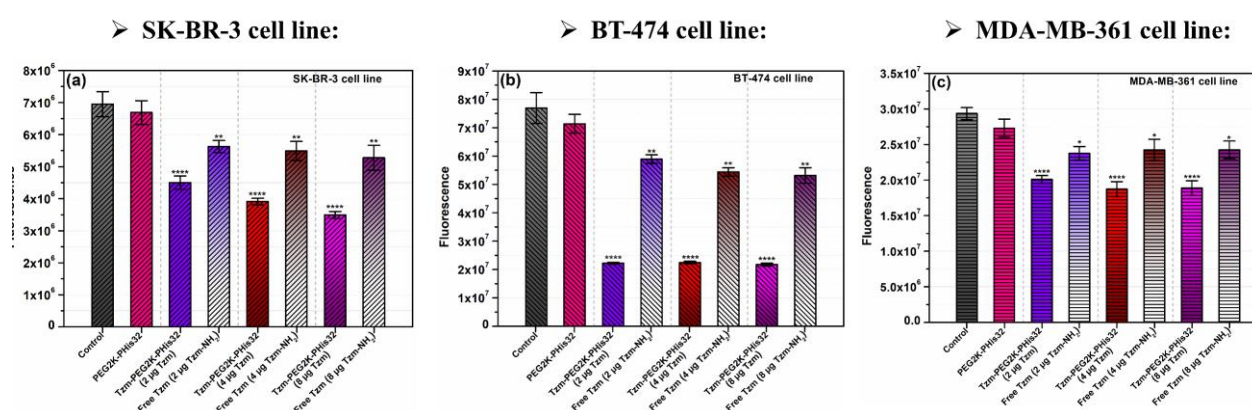
Figure III.23. Cytotoxicity of nonfunctionalized micelles, those functionalized with three different concentrations of Tzm and free Tzm at three concentrations equal to those used for functionalization, on three breast cancer-specific tumor cell lines with response to Tzm (SK-BR-3, BT-474, unidirectional ANOVA, **p < 0.01; ****p < 0.0001) and intermediate response (MDA-MB-361, unidirectional ANOVA, *p < 0.5; ****p < 0.0001).

The addition of Tzm to the surface of micelles (Tzm-PEG2K-PHis32) resulted in a significant decrease in cell viability in all three cell types, with significantly lower viability than that achieved with free Tzm at all three concentrations tested (according to **figure III.23.**).

This effect on cell viability given by the covalent binding of Tzm to the surface of micelles was also obtained on 3D cell cultures (spheroids) (**figure III.24.**).
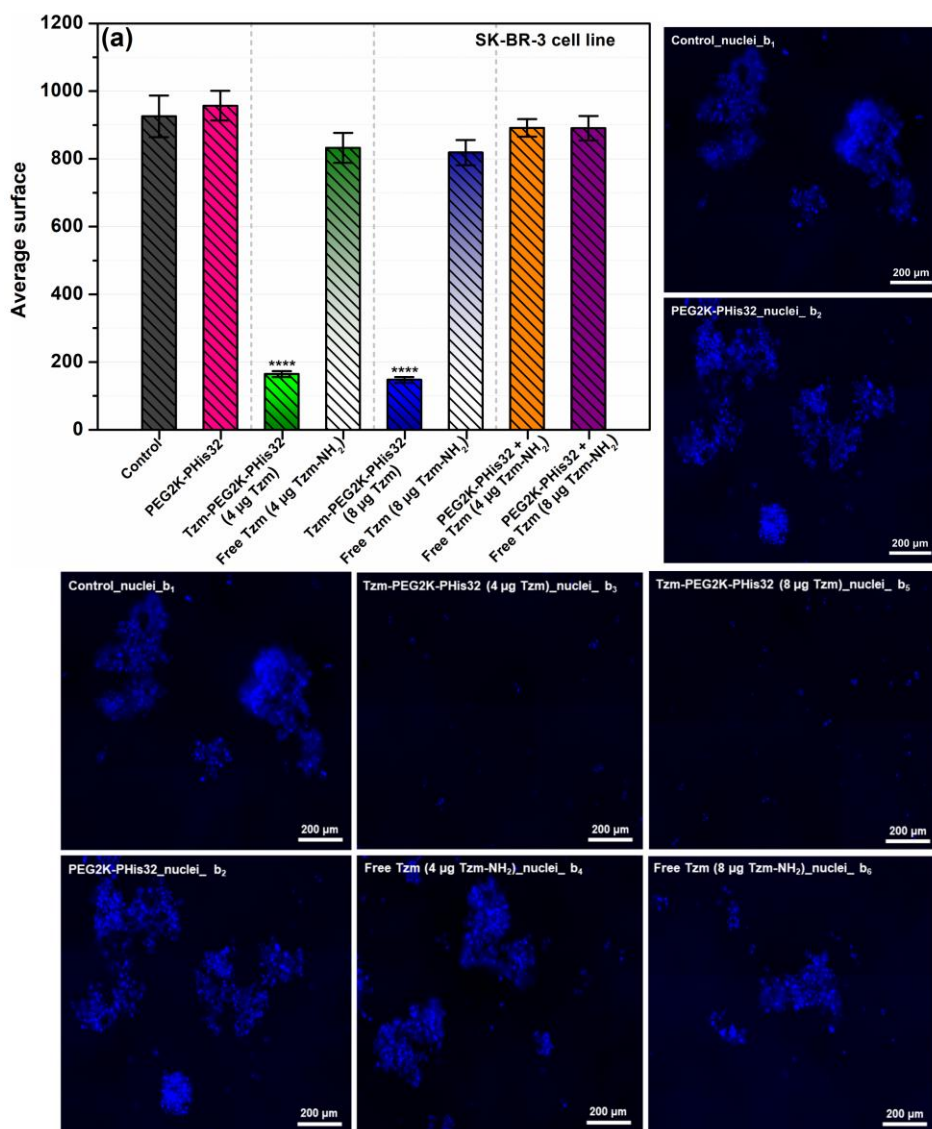
Figure III.24. Efficacy of micelles (non-functionalized and functionalized with Tzm), free Tzm and mixed treatment (non-functionalized micelles + free Tzm) on SK-BR-3 cell cultures of type 3D: a) variation of mean spheroid surfaces after 72 hours of treatment; (b1-8) representative fluorescence images to show spheroids disassembly upon interaction with micelles functionalized with Tzm compared to controls (unidirectional ANOVA, ****$p < 0,0001$).

The efficacy of micelles was determined by morphological analysis of spheroids (cell nuclei were stained with a fluorescent compound, which when it binds specifically to nuclear DNA leads to a blue coloration) after treatment by measuring their surface. Thus, analysing **figure III.24. (a, b3, b5)**, it can be noted that in the case of the SK-BR-3 cell line, spheroids were affected by micelles functionalised with Tzm (Tzm-PEG2K-PHis32 (4 µg Tzm) and Tzm-PEG2K-PHis32 (8 µg Tzm)), with significant reduction of their mean surface area compared to the free Tzm tested at the two concentrations (**figure III.24.b3, b5**). Nonfunctionalized micelles, free Tzm (4 µg and 8 µg) and mixed treatment had no significant effect on spheroids after incubation for 72 hours. The results obtained on the SK-BR-3 cell line were also obtained on the MDA-MB-361 cell line (which shows intermediate response to Tzm).

GENERAL CONCLUSIONS

The results obtained within the doctoral thesis entitled **"New approaches for the development of functionalized polymeric nanosystems with applications in nanomedicine"** led to a series of general conclusions related to each chapter of the second part of this thesis including personal results, as follows:

Chapter II:

➢ Magnetic nanoparticles (MNPs) with an average diameter of about 9 nm obtained by TEM were synthesized, using for synthesis the method of coprecipitation of iron(II) and (III) salts in basic medium.

➢ An ATRP polymerization initiator based on L-dopamine was synthesized, and its structure was highlighted by magnetic resonance spectroscopy. The initiator was attached by covalent bonds to the surface of magnetic nanoparticles.

➢ The polymerization of the HEMA monomer on the surface of the synthesized magnetic nanoparticles was achieved by SI-ATRP polymerization mechanism. HEMA polymerization was initiated by the presence of the appropriate initiator previously grafted onto the MNP surface.

➢ Folic acid was covalently bound (involving two different concentrations) to free hydroxyl groups on the side chain of each monomer structural unit (HEMA) in the presence of a carbodiimide-type catalyst.

➢All chemical structures obtained were physicochemical characterized by methods specific to solid state characterization (FTIR, Raman, XRD, TGA/DTG, DSC, VSM, TEM, STEM) or liquid such as DLS and zeta potential. Following the morphological analysis of nanoparticles obtained by STEM, it can be concluded that the average diameter of PHEMA-coated nanoparticles was 18.9 nm, those functionalized with the first concentration of FA was 17.7 nm, while the second concentration of FA had an average diameter of 15.7 nm.

➢ Folic acid quantification was achieved by UV-Vis spectroscopy using the calibration curve method (31.5 µg FA / mg MNP-PHEMA-FA1 and 83.5 µg FA / mg MNP-PHEMA-FA2).

➢ The magnetic nanoparticles coated with folic acid-functionalized PHEMA chains were biocompatible on the normal NHDF cell line, thus not affecting the viability of the MCF-7, HeLa and HepG2 tumour cell lines, respectively.

➢ Knowing that cancer cell lines (MCF-7, HeLa, HepG2) overexpress folate receptors on their membrane surface compared to normal cells (NHDF), it was demonstrated that cellular uptake of the functionalized nanocarrier with folic acid was significantly higher than

nonfunctionalized nanoparticles, demonstrated by higher values in absorbance on cancer cell lines compared to normal. This absorption was demonstrated by quantification of intracellular iron using the thiocyanate method.

➢ Atomic absorption spectroscopy concluded that increasing the concentration of folic acid used to functionalize magnetic nanoparticles decorated with PHEMA chains leads to an increase in cell uptake in cancer cells (MCF-7) compared to normal cells (NHDF).

➢ Because the saturation magnetization of nanoparticles decorated with FA-functionalized PHEMA chains had a value of over 7 emu / g (minimum value accepted for using an MRI imaging contrast system), the possibility of these nanoparticles to be used as contrast agents in MRI imaging was highlighted.

➢ To demonstrate the versatility of ATRP polymerization, using the same magnetic nanoparticles decorated with the initiator synthesized and attached to the surface of MNPs, three methacrylate-type monomers (HEMA, PEGMA6 and PEGMA10), with different side chain lengths of monomeric units, were polymerized by SI-ATRP polymerization mechanism.

➢ The three polymers grafted onto the surface of MNPs (PHEMA, PPEGMA6 and PPEGMA10) were functionalized with a folic acid antimetabolite, methotrexate (MTX), which exhibits dual functionality of both targeting folate receptors and therapeutic effect by inhibiting an enzyme involved in cancer cell division.

➢ All synthesis steps to obtain the three magnetic nanoparticles decorated with the three polymers functionalized with MTX were physicochemical characterized by different methods (FTIR, TGA/DTG, DSC, VSM, DLS). Spherical nanoparticles with average diameters of 17.12 nm, 15.30 nm, 17.16 nm corresponding to MNP-PHEMA-MTX, MNP-PPEGMA6-MTX and MNP-PPEGMA10-MTX samples were obtained, respectively.

➢ MTX was quantified by UV-Vis spectroscopy using the calibration curve method.

➢ Magnetic nanoparticles decorated with polymers and MTX were biocompatible on the normal HGF cell lineage.

➢ MNPs coated with the three MTX-functionalized polymers (MNP-PHEMA-MTX, MNP-PPEGMA6-MTX, MNP-PPEGMA10-MTX) showed a toxic effect on the MCF-7 cell line (breast adenocarcinoma), an effect demonstrated by lowering cell viability below the threshold of 70%, significantly greater decrease than free drug (free MTX).

Following the conclusions obtained in Chapter II, the recommendation to use magnetic nanoparticles decorated with methacrylate-type polymers as theranostic nanoplatforms is outlined. This promising prospect is supported by the presence of a magnetic nucleus, which facilitates their application in imaging, and their size below 30 nm, which adds a crucial aspect.

These nanoplatforms also demonstrate the ability to transport drugs. A significant advantage of using ATRP-type polymerization lies in the possibility of obtaining double layers of polymers, paving the way for the functionalization of the first layer with a drug and the second with a targeting molecule. These essential characteristics underline the considerable potential of nanoparticles in cancer therapy. However, it is imperative that further research is carried out to highlight the efficacy of this nanocarrier in vivo tests, representing a crucial step before advancing to clinical trials on humans.

Chapter III:

➤ Three polyethylene glycol-polyhistidine (PEG - PHis) copolymers with a PEG chain length of 2 kDa and different PHis chain lengths (20, 26 and 32 repetitive monomer units of histidine) were synthesized by SPPS technique.

➤ The critical micelle concentration of the three copolymers was determined and it was concluded that an increase in the PHis chain leads to a decrease in the CMC value.

➤ The copolymers were assembled in unloaded micelles and loaded with DOX (used as a model compound due to its fluorescence leading to an easy quantification method) of the core-shell type in aqueous solutions with PBS at physiological pH.

➤ Unloaded micelles were morphologically analysed by DLS in aqueous solutions at physiological pH, resulting in an increase in polyhistidine chain length leading to an increase in the hydrodynamic diameter of micelles, an increase also observed in DOX-loaded micelles.

➤ The STEM technique highlighted core-shell structures and the influence of PHis sequence length in the formation of micellar systems. Increasing the length of the PHis chain leads to a decrease in the diameter of the micelles (unloaded and loaded), a decrease attributed to compaction of PHis chains (the longer the PHis chain length, the greater the compaction).

➤ Quantification of DOX loaded into micelles was performed by fluorescence, using the calibration curve method, encapsulation efficiency and drug loading increased with increasing PHis chain.

➤ Following studies of controlled release of DOX from micelles at physiological pH, it was observed that it is released from micelles in a small percentage, which leads to the fact that at this pH the micelles are stable and hold the DOX loaded, but with decreasing pH, the concentration of DOX released increases, reaching 50% at a pH = 6.5 within 10 hours.

➤ The viability of breast cancer-specific MDA-MB-231 cells treated with unloaded micellar solutions did not significantly decrease compared to controls (untreated cells) after 72 hours, while those loaded with DOX resulted in a decrease in cell viability, but not large enough

compared to free DOX administration, leading to the idea that DOX-loaded micelles release the drug slowly with decreasing pH values.

The conclusions of the first study in Chapter III, demonstrate the versatility of varying the length of the polyhistidine chain with influencing the physicochemical properties of the formed micelles, ensuring the transport and release of a drug into tumour extracellular environment. Corroborating the results of the study, it can be concluded that micelles based on PEG-PHis diblock copolymers can be recommended for the transport of release drugs into the tumour extracellular environment.

Conclusions of the second Chapter III study:

➢ In the first stage, the H_2N-PEG-2000-Mal-Cis-(His)32 copolymer was functionalized with 32 histidine units with a maleimide linker (Linker-PEG-2000-Mal-Cis-(His)32) and commercial trastuzumab (Tzm-NH_2) with thiol groups, with the help of Traut agent (transformation of free amine groups into free thiol groups). Thiol groups in the structure of thiolated Tzm (Tzm-SH) were quantified using Ellman's agent, involving UV-Vis spectroscopy.

➢ In the next step, maleimide groups in Linker-PEG2K-PHis32 micelles were reacted with SH groups in Tzm-SH, resulting in a Tzm-PEG2K-PHis32 micellar system grafted with Tzm molecules.

➢ The binding of Tzm-SH to Linker-PEG2K-PHis32 micelles was demonstrated by modifying the zeta potential of the resulting micelles.

➢ Morphologically, the micelles were analysed by STEM, where the surface of micelles loaded with Tzm molecules was highlighted.

➢ Assembly in micelles at pH = 7,4 and disassembly was evidenced by the NTA technique (Brownian motion of micelles).

➢ Stability studies in the presence of BSA indicated that non-functionalized micelles were completely disassembled, while those functionalized with Tzm remained stable over a period of 72 hours.

➢ The micelles were biocompatible on the normal HGF cell line.

➢ In the case of *in vitro* studies on three breast cancer-specific cancer cell lines (2D and 3D cell cultures) micelles functionalized with Tzm led to a decrease in cell viability compared to free Tzm, an effect accentuated by spheroid damage in 3D cultures (Free tzm did not affect spheroids).

The results of this study conclude that binding of Tzm to micelles leads to a significantly higher toxic effect than free Tzm, but at the same time presents insight into the mechanism of action of micelles functionalized with monoclonal antibody on breast cancer-specific cancer cells.

DISSEMINATION OF RESULTS

Articles published in ISI indexed scientific journals, the results of which made up the content of the doctoral thesis:

1. Ghiarasim, R., Simionescu, N., Coroaba, A., Uritu, C. M., Marangoci, N. L., Ibanescu, S. A., & Pinteala, M. (**2022**). SI-ATRP Decoration of Magnetic Nanoparticles with PHEMA and Post-Polymerization Modification with Folic Acid for Tumor Cells' Specific Targeting. *International Journal of Molecular Sciences*, 23(1), 155 (**IF = 6,2**).

2. Ghiarasim, R., Tiron, C. E., Tiron, A., Dimofte, M. G., Pinteala, M., & Rotaru, A. (**2022**). Solid-Phase Synthesized Copolymers for the Assembly of pH-Sensitive Micelles Suitable for Drug Delivery Applications. *Nanomaterials*, 12(11), 1798 (**IF = 5,4**).

3. Morarasu, S., Morarasu, B. C., **Ghiarasim, R.**, Coroaba, A., Tiron, C., Iliescu, R., & Dimofte, G. M. (**2022**). Targeted cancer therapy Via ph-functionalized nanoparticles: A scoping review of methods and outcomes. *Gels*, 8(4), 232 (**IF = 5.2**).

4. **Ghiarasim, R.**, Varganici, C.D., Simionescu, N., & Pinteala, M.(**2024**). Synthesis of magnetic nanoparticles coated with three methacrylate-type polymers obtained by SI-ATRP functionalized with methotrexate for antineoplastic activity on MCF-7 cells. *ACS Polymers Au*, **Forthcoming publication** (**IF = 3,9**).

Articles published in ISI indexed scientific journals, whose results were related to the topic of the doctoral thesis (these results were not included in the content of the thesis):

1. Sardaru, M. C., Rosca, I., Morariu, S., Ursu, E. L., **Ghiarasim, R.**, & Rotaru, A. (**2021**). Injectable Thixotropic β–Cyclodextrin–Functionalized Hydrogels Based on Guanosine Quartet Assembly. *International Journal of Molecular Sciences*, 22(17), 9179 (**IF = 6,2**).

During his doctoral studies, Ph.D. student Răzvan Ghiarasim was a member of the implementation team of the following projects:

1. „Modular approach to nanoparticle synthesis processes coated with multifunctional polymers for nanomedical applications (**ModNanoMPol**)", PN-III-P1-1.1-TE-2019-0922.

2. „Restore HER2 dependent sensibility using AXL inhibitors packed in pH dependent nanostructures (**NanoHER2Restore**)", EEA-RO-NO-2018-0246.

Research internships / mobilities carried out during doctoral studies:

1. Research internship at Scientific Services Company Otava Ltd., Kiev, Ukraine, between 19.09.2021 - 18.10.2021 (one month) within the project H2020-MSCA-RISE-2019, *NoBiasFluors* No 872331.

2. Research internship at Naukovo Vyrobnichyj Kooperatyv Lectinotest, Lviv, Ukraine, between 30.06.2023 - 29.08.2023 (two months) within the project H2020-MSCA-RISE-2019, NoBiasFluors No 872331.

3. Research internship at Estonian University of Life Sciences from 01.10.2023 to 31.10.2023 (one month) within the project HORIZON-MSCA-2021-SE-01, *VOLATEVS, No 101086360.*

4. Mobility for transporting series of samples and conducting experiments (24.10.2022 - 29.10.2022, 10.09.2023 - 16.09.2023, 03.03.2024 - 11.03.2024) to a project partner *Restore HER2 dependent sensitivity using Axl inhibitors packed in ph dependent nanostructures* - EEA-RO-NO-2018-0246(NANOHER2RESTORE) from Oslo, Norway.

Participation in national / international scientific conferences:

Oral communications:

1. Răzvan Ghiarasim, Sorin-Alexandru Ibănescu, Narcisa-Laura Marangoci, Adina Coroabă, Natalia Simionescu, Mariana Pinteală. ,,Synthesis and characterization of magnetite nanoparticles coated with a double layer of polymer obtained by SI-ATRP functionalized with the targeting molecule and drug with the property of cleavage in acid pH''. Online communication at the 2nd International Conference on Polymer Science and Composite Materials, Barcelona, Spain, July 05th - 07th, 2021.

2. Răzvan Ghiarasim, Sorin-Alexandru Ibănescu, Cristian-Dragos Varganici, Natalia Simionescu and Mariana Pinteală. ,,Synthesis of magnetic nanoparticles coated with three methacrylate-type polymers obtained by SI-ATRP functionalized with methotrexate for antineoplastic activity on HeLa cells''. Oral communication at the 5th Autumn School on Physics of Advanced Materials (PAMS-5) September 8 - 15, 2022, in Dubrovnik, Croatia.

3. Răzvan Ghiarasim, Crina Elena Tiron, Adrian Tiron, Mihail-Gabriel Dimofte, Mariana Pinteală and Alexandru Rotaru. ,,Solif-phase synthesis copolymers for the assembly of pH-sensitive micelles suitable fro drug delivery applications''. Oral communication at the National Conference of Chemistry, CNChim-2022, XXXVI edition, 04 - 07 October 2022, Călimănești - Căciulata, Vâlcea County, Romania.

4. Răzvan Ghiarasim, oral presentation „Poly(ethylene glycol)-polyhistidine copolymers synthesized by solid-phase peptide synthesis: self-assembly into pH-responsive micelles for targeted drug delivery applications", 12th International Symposium "Polyimides & High-Performance Materials" stePI12, 4 - 7 june, 2023,Montpellier Sud de France, France.

Posters:

1. Răzvan Ghiarasim, Sorin-Alexandru Ibănescu, Narcisa-Laura Marangoci, Adina Coroabă, Natalia Simionescu, Mariana Pinteală. „Synthesis of magnetic nanoparticles coated with pHEMA functionalized with doxorubicin and folic acid for cancer therapy". Poster at the 23rd International Conference 19 - 22 August 2021 Burgas, Bulgaria, Materials, Methods & Technologies.

2. Răzvan Ghiarasim, Lucian Bahrin, Bogdan Crăciun, Crina Tiron, Gabriel Dimofte and Mariana Pinteală. „Synthesis, characterization, and preliminary testing of doxorubicin loaded poly(L-histidine)-PEG copolymer micelles as pH sensitive drug delivery systems". Poster at the 23rd International Conference 19 - 22 August 2021 Burgas, Bulgaria, Materials, Methods & Technologies.

3. Răzvan Ghiarasim, Sorin-Alexandru Ibănescu, Narcisa-Laura Marangoci, Adina Coroabă, Natalia Simionescu and Mariana Pinteală. "Magnetic nanoparticles decorated with poly(2-hydroxyethyl methacrylate) functionalized with folic acid as a smart targeting nanocarrier by overexpressing the folate receptor on the surface of tumor cells." Scientific communication session of students, master, and doctoral students "Chemistry – Open frontier to knowledge", twelfth edition, Iasi, November 11 - 12, 2021, Organizer: "Alexandru Ioan Cuza" University of Iasi, Faculty of Chemistry.

4. Răzvan Ghiarasim, Crina Elena Tiron, Gabriel Dimofte, Mariana Pinteală and Alexandru Rotaru. „Solid phase synthesized polyhistidine-based copolymers for the assembly of pH-sensitive micelles suitable for drug delivery in cancer extracellular environment". Poster at the 7th International Congress on Biomaterials and Biosensors (BIOMATSEN) International Conference, 22-28 April 2022, Mugla, Turkey.

5. Răzvan Ghiarasim, Crina Elena Tiron, Adrian Tiron, Mihail-Gabriel Dimofte, Mariana Pinteală. „Copolymers-based micelles obtained by solid-phase synthesis with controlled disassembly property triggered by pH variation for drug delivery applications". Poster at 14th International Conference on Physics of Advanced Materials (IPCAM-14), 8 - 15 September 2022, Dubrovnik, Croatia.

6. Răzvan Ghiarasim, Crina Elena Tiron, Adrian Tiron, Mihail-Gabriel Dimofte, Alexandru Rotaru, and Mariana Pinteală, poster, "Studies of polyhistidine-polyethylene glycol copolymers for the assembly of pH-sensitive micelles able to covalently attach trastuzumab for efficient breast cancer treatment.", Frontiers in Polymer Science 2023 (POLY2023), 29 May - 1 June 2023, Gothenburg, Sweden.

7. Răzvan Ghiarasim, Cristian-Dragoș Varganici, Natalia Simionescu, Sorin-Alexandru Ibănescu and Mariana Pinteală, poster, " Three exemples of polymers obtained by SI-ATRP on magnetic nanoparticles surface with post-polymerization modification with methotrexate as efficient drug carriers for antineoplastic activity on MCF-7 cell line.", Frontiers in Polymer Science 2023 (POLY2023), 29 May - 1 June 2023, Gothenburg, Sweden.

SELECTED BIBLIOGRAPHY

Adam-Artigues, A., Arenas, E.J., Martínez-Sabadell, A., Brasó-Maristany, F., Cervera, R., Tormo, E., Hernando, C., Martínez, M.T., Carbonell-Asins, J., Simón, S., Poveda, J., Moragón, S., Zazo, S., Martínez, D., Rovira, A., Burgués, O., Rojo, F., Albanell, J., Bermejo, B., Lluch, A., Prat, A., Arribas, J., Eroles, P. and Cejalvo, J.M. (2022) 'Targeting HER2-AXL heterodimerization to overcome resistance to HER2 blockade in breast cancer', *Science Advances*, 8(20).

Anghelache, M., Turtoi, M., Petrovici, A.R., Fifere, A., Pinteala, M. and Calin, M. (2021) 'Development of Dextran-Coated Magnetic Nanoparticles Loaded with Protocatechuic Acid for Vascular Inflammation Therapy', *Pharmaceutics*, 13(9), p. 1414.

Arruebo, M., Vilaboa, N., Sáez-Gutierrez, B., Lambea, J., Tres, A., Valladares, M. and González-Fernández, Á. (2011) 'Assessment of the Evolution of Cancer Treatment Therapies', *Cancers*, 3(3), pp. 3279–3330.

Baek, S., Singh, R.K., Khanal, D., Patel, K.D., Lee, E.-J., Leong, K.W., Chrzanowski, W. and Kim, H.-W. (2015) 'Smart multifunctional drug delivery towards anticancer therapy harmonized in mesoporous nanoparticles', *Nanoscale*, 7(34), pp. 14191–14216.

Barbey, R., Lavanant, L., Paripovic, D., Schüwer, N., Sugnaux, C., Tugulu, S. and Klok, H.-A. (2009) 'Polymer Brushes via Surface-Initiated Controlled Radical Polymerization: Synthesis, Characterization, Properties, and Applications', *Chemical Reviews*, 109(11), pp. 5437–5527.

Beagan, A.M., Alghamdi, A.A., Lahmadi, S.S., Halwani, M.A., Almeataq, M.S., Alhazaa, A.N., Alotaibi, K.M. and Alswieleh, A.M. (2020) 'Folic Acid-Terminated Poly(2-Diethyl Amino Ethyl Methacrylate) Brush-Gated Magnetic Mesoporous Nanoparticles as a Smart Drug Delivery System', *Polymers*, 13(1), p. 59.

Beers, K.L., Boo, S., Gaynor, S.G. and Matyjaszewski, K. (1999) 'Atom Transfer Radical Polymerization of 2-Hydroxyethyl Methacrylate', *Macromolecules*, 32(18), pp. 5772–5776.

Behrendt, R., White, P. and Offer, J. (2016) 'Advances in Fmoc solid-phase peptide synthesis', *Journal of Peptide Science*, 22(1), pp. 4–27.

Bondalapati, S., Jbara, M. and Brik, A. (2016) 'Expanding the chemical toolbox for the synthesis of large and uniquely modified proteins', *Nature Chemistry*, 8(5), pp. 407–418.

Carrillo-Castillo, T.D., Castro-Carmona, J.S., Luna-Velasco, A. and Zaragoza-Contreras, E.A. (2020) 'pH-responsive polymer micelles for methotrexate delivery at tumor microenvironments', *e-Polymers*, 20(1), pp. 624–635.

Chen, M., Chen, C., Shen, Z., Zhang, X., Chen, Y., Lin, F., Ma, X., Zhuang, C., Mao, Y., Gan, H., Chen, P., Zong, X. and Wu, R. (2017) 'Extracellular pH is a biomarker enabling detection of breast cancer and liver cancer using CEST MRI', *Oncotarget*, 8(28), pp. 45759–45767.

Cipolla, D., Wu, H., Salentinig, S., Boyd, B., Rades, T., Vanhecke, D., Petri-Fink, A., Rothin-Rutishauser, B., Eastman, S., Redelmeier, T., Gonda, I. and Chan, H.K. (2016) 'Formation of drug nanocrystals under nanoconfinement afforded by liposomes', *RSC Advances*, 6(8), pp. 6223–6233.

Crezee, J., Franken, N.A.P. and Oei, A.L. (2021) 'Hyperthermia-Based Anti-Cancer Treatments', *Cancers*, 13(6), p. 1240.

El-Faham, A. and Albericio, F. (2011) 'Peptide Coupling Reagents, More than a Letter Soup', *Chemical Reviews*, 111(11), pp. 6557–6602.

Ellman, G.L. (1959) 'Tissue sulfhydryl groups', *Archives of Biochemistry and Biophysics*, 82(1), pp. 70–77.

Ghiarasim, R., Simionescu, N., Coroaba, A., Uritu, C.M., Marangoci, N.L., Ibanescu, S.-A. and Pinteala, M. (2021) 'SI-ATRP Decoration of Magnetic Nanoparticles with PHEMA and Post-Polymerization Modification with Folic Acid for Tumor Cells' Specific Targeting', *International Journal of Molecular Sciences*, 23(1), p. 155.

Ghiarasim, R., Tiron, C.E., Tiron, A., Dimofte, M.-G., Pinteala, M. and Rotaru, A. (2022) 'Solid-Phase Synthesized Copolymers for the Assembly of pH-Sensitive Micelles Suitable for Drug Delivery Applications', *Nanomaterials*, 12(11), p. 1798.

Gradishar, W.J., O'Regan, R., Rimawi, M.F., Nordstrom, J.L., Rosales, M.K. and Rugo, H.S. (2023) 'Margetuximab in HER2-positive metastatic breast cancer', *Future Oncology*, 19(16), pp. 1099–1112.

Guimarães, D., Lager, F., Renault, G., Guezguez, J., Burnet, M., Cunha, J., Cavaco-Paulo, A. and Nogueira, E. (2022) 'Folate-Targeted Liposomal Formulations Improve Effects of Methotrexate in Murine Collagen-Induced Arthritis', *Biomedicines*, 10(2), p. 229.

Guimarães, D., Noro, J., Loureiro, A., Lager, F., Renault, G., Cavaco-Paulo, A. and Nogueira, E. (2020) 'Increased Encapsulation Efficiency of Methotrexate in Liposomes for Rheumatoid Arthritis Therapy', *Biomedicines*, 8(12), p. 630.

Gul, S., Khan, S.B., Rehman, I.U., Khan, M.A. and Khan, M.I. (2019) 'A Comprehensive Review of Magnetic Nanomaterials Modern Day Theranostics', *Frontiers in Materials*, 6 Frontiers Media S.A., p. 179. Available at: 10.3389/FMATS.2019.00179/BIBTEX (Accessed: 4 December 2021).

Gupta, A.K. and Gupta, M. (2005) 'Cytotoxicity suppression and cellular uptake enhancement of surface modified magnetic nanoparticles', *Biomaterials*, 26(13), pp. 1565–1573.

Gupta, J., Bhargava, P. and Bahadur, D. (2014) 'Methotrexate conjugated magnetic nanoparticle for targeted drug delivery and thermal therapy', *Journal of Applied Physics*, 115(17).

Hu, J., Miura, S., Na, K. and Bae, Y.H. (2013) 'pH-responsive and charge shielded cationic micelle of poly(l -histidine)- block -short branched PEI for acidic cancer treatment', *Journal of Controlled Release*, 172(1), pp. 69–76.

Israel, L.L., Galstyan, A., Holler, E. and Ljubimova, J.Y. (2020) 'Magnetic iron oxide nanoparticles for imaging, targeting and treatment of primary and metastatic tumors of the brain', *Journal of Controlled Release*, 320 Elsevier, pp. 45–62. Available at: 10.1016/j.jconrel.2020.01.009 (Accessed: 4 December 2021).

Jahangirian, H., Kalantari, K., Izadiyan, Z., Rafiee-Moghaddam, R., Shameli, K. and Webster, T.J. (2019) '<p>A review of small molecules and drug delivery applications using gold and iron nanoparticles</p>', *International Journal of Nanomedicine*, Volume 14, pp. 1633–1657.

Jain, N., Smith, S.W., Ghone, S. and Tomczuk, B. (2015) 'Current ADC Linker Chemistry', *Pharmaceutical Research*, 32(11), pp. 3526–3540.

Kim, G.M., Bae, Y.H. and Jo, W.H. (2005) 'pH-induced Micelle Formation of Poly(histidine-co -phenylalanine)- *block* -Poly(ethylene glycol) in Aqueous Media', *Macromolecular Bioscience*, 5(11), pp. 1118–1124.

Kohler, N., Sun, C., Fichtenholtz, A., Gunn, J., Fang, C. and Zhang, M. (2006) 'Methotrexate-Immobilized Poly(ethylene glycol) Magnetic Nanoparticles for MR Imaging and Drug Delivery', *Small*, 2(6), pp. 785–792.

Kohler, N., Sun, C., Wang, J. and Zhang, M. (2005) 'Methotrexate-Modified Superparamagnetic Nanoparticles and Their Intracellular Uptake into Human Cancer Cells', *Langmuir*, 21(19), pp. 8858–8864.

Kulhari, H., Pooja, D., Shrivastava, S., Kuncha, M., Naidu, V.G.M., Bansal, V., Sistla, R. and Adams, D.J. (2016) 'Trastuzumab-grafted PAMAM dendrimers for the selective delivery of anticancer drugs to HER2-positive breast cancer', *Scientific Reports*, 6(1), p. 23179.

Lee, E.S., Shin, H.J., Na, K. and Bae, Y.H. (2003a) 'Poly(l-histidine)–PEG block copolymer micelles and pH-induced destabilization', *Journal of Controlled Release*, 90(3), pp. 363–374.

Lee, E.S., Shin, H.J., Na, K. and Bae, Y.H. (2003b) 'Poly(l-histidine)–PEG block copolymer micelles and pH-induced destabilization', *Journal of Controlled Release*, 90(3), pp. 363–374.

Leeman, M., Choi, J., Hansson, S., Storm, M.U. and Nilsson, L. (2018) 'Proteins and antibodies in serum, plasma, and whole blood—size characterization using asymmetrical flow field-flow fractionation (AF4)', *Analytical and Bioanalytical Chemistry*, 410(20), pp. 4867–4873.

Li, M., Neoh, K.-G., Wang, R., Zong, B.-Y., Tan, J.Y. and Kang, E.-T. (2013) 'Methotrexate-conjugated and hyperbranched polyglycerol-grafted Fe3O4 magnetic nanoparticles for targeted anticancer effects', *European Journal of Pharmaceutical Sciences*, 48(1–2), pp. 111–120.

Li, S., Sun, Z., Meng, X., Deng, G., Zhang, J., Zhou, K., Li, W., Zhou, L., Gong, P. and Cai, L. (2018) 'Targeted Methotrexate Prodrug Conjugated With Heptamethine Cyanine Dye Improving Chemotherapy and Monitoring Itself Activating by Dual-Modal Imaging', *Frontiers in Materials*, 5.

Lungoci, A.-L., Turin-Moleavin, I.-A., Corciova, A., Mircea, C., Arvinte, A., Fifere, A., Marangoci, N.L. and Pinteala, M. (2019) 'Multifunctional magnetic cargo-complexes with radical scavenging properties', *Materials Science and Engineering: C*, 94, pp. 608–618.

Marega, R., Karmani, L., Flamant, L., Nageswaran, P.G., Valembois, V., Masereel, B., Feron, O., Borght, T. Vander, Lucas, S., Michiels, C., Gallez, B. and Bonifazi, D. (2012) 'Antibody-functionalized polymer-coated gold nanoparticles targeting cancer cells: an in vitro and in vivo study', *Journal of Materials Chemistry*, 22(39), p. 21305.

von Minckwitz, G., Huang, C.-S., Mano, M.S., Loibl, S., Mamounas, E.P., Untch, M., Wolmark, N., Rastogi, P., Schneeweiss, A., Redondo, A., Fischer, H.H., Jacot, W., Conlin, A.K., Arce-Salinas, C., Wapnir, I.L., Jackisch, C., DiGiovanna, M.P., Fasching, P.A., Crown, J.P., Wülfing, P., Shao, Z., Rota Caremoli, E., Wu, H., Lam, L.H., Tesarowski, D., Smitt, M., Douthwaite, H., Singel, S.M. and Geyer, C.E. (2019) 'Trastuzumab Emtansine for Residual Invasive HER2-Positive Breast Cancer', *New England Journal of Medicine*, 380(7), pp. 617–628.

Modi, S., Jacot, W., Yamashita, T., Sohn, J., Vidal, M., Tokunaga, E., Tsurutani, J., Ueno, N.T., Prat, A., Chae, Y.S., Lee, K.S., Niikura, N., Park, Y.H., Xu, B., Wang, X., Gil-Gil, M., Li, W., Pierga, J.-Y., Im, S.-A., Moore, H.C.F., Rugo, H.S., Yerushalmi, R., Zagouri, F., Gombos, A., Kim, S.-B., Liu, Q., Luo, T., Saura, C., Schmid, P., Sun, T., Gambhire, D., Yung, L., Wang, Y., Singh, J., Vitazka, P., Meinhardt, G., Harbeck, N. and Cameron, D.A. (2022) 'Trastuzumab Deruxtecan in Previously Treated HER2-Low Advanced Breast Cancer', *New England Journal of Medicine*, 387(1), pp. 9–20.

Mohammed, M.O., Alkubaisi, H.M.M. and Haj, N.Q. (2020) 'A new prodrug and bioactivity evaluation of methotrexate based on Chitosan', *Heliyon*, 6(6), p. e04223.

Nahta, R., Yu, D., Hung, M.-C., Hortobagyi, G.N. and Esteva, F.J. (2006) 'Mechanisms of Disease: understanding resistance to HER2-targeted therapy in human breast cancer', *Nature Clinical Practice Oncology*, 3(5), pp. 269–280.

Najafian, N., Shanehsazzadeh, S., Hajesmaeelzadeh, F., Lahooti, A., Gruettner, C. and Oghabian, M.A. (2015) 'Effect of Functional Group and Surface Charge of PEG and Dextran-Coated USPIO as a Contrast Agent in MRI on Relaxivity Constant', *Applied Magnetic Resonance*, 46(6), pp. 685–692.

Nanda, J.S. and Lorsch, J.R. (2014) 'Labeling a Protein with Fluorophores Using NHS Ester Derivitization', in *Methods in Enzymology*. , pp. 87–94.

Nguyen, H.T., Tran, T.H., Thapa, R.K., Phung, C.D., Shin, B.S., Jeong, J.-H., Choi, H.-G., Yong, C.S. and Kim, J.O. (2017) 'Targeted co-delivery of polypyrrole and rapamycin by trastuzumab-conjugated liposomes for combined chemo-photothermal therapy', *International Journal of Pharmaceutics*, 527(1–2), pp. 61–71.

Nosrati, H., Salehiabar, M., Davaran, S., Danafar, H. and Manjili, H.K. (2018) 'Methotrexate-conjugated L-lysine coated iron oxide magnetic nanoparticles for inhibition of MCF-7 breast cancer cells', *Drug Development and Industrial Pharmacy*, 44(6), pp. 886–894.

Peng, J., Chen, J., Xie, F., Bao, W., Xu, H., Wang, H., Xu, Y. and Du, Z. (2019) 'Herceptin-conjugated paclitaxel loaded PCL-PEG worm-like nanocrystal micelles for the combinatorial treatment of HER2-positive breast cancer', *Biomaterials*, 222, p. 119420.

Poletto, G., Evangelista, L., Venturini, F., Gramegna, F., Seno, F., Moro, S., Vettor, R., Realdon, N. and Cecchin, D. (2022) 'Nanoparticles and Radioisotopes: A Long Story in a Nutshell', *Pharmaceutics*, 14(10), p. 2024.

Rowe, M.D., Chang, C.-C., Thamm, D.H., Kraft, S.L., Harmon, J.F., Vogt, A.P., Sumerlin, B.S. and Boyes, S.G. (2009) 'Tuning the Magnetic Resonance Imaging Properties of Positive Contrast Agent Nanoparticles by Surface Modification with RAFT Polymers', *Langmuir*, 25(16), pp. 9487–9499.

Samaritoni, J., Martynow, J., O'Donnell, M. and Scott, W. (2018) 'Preparation and Use of a General Solid-Phase Intermediate to Biomimetic Scaffolds and Peptide Condensations', *Molecules*, 23(7), p. 1762.

Schena, E., Saccomandi, P. and Fong, Y. (2017) 'Laser Ablation for Cancer: Past, Present and Future', *Journal of Functional Biomaterials*, 8(2), p. 19.

Sharma, R., Borah, S.J., Bhawna, Kumar, S., Gupta, A., Singh, P., Goel, V.K., Kumar, R. and Kumar, V. (2022) 'Functionalized Peptide-Based Nanoparticles for Targeted Cancer Nanotherapeutics: A State-of-the-Art Review', *ACS Omega*, 7(41), pp. 36092–36107.

Singh, U., Morya, V., Rajwar, A., Chandrasekaran, A.R., Datta, B., Ghoroi, C. and Bhatia, D. (2020) 'DNA-Functionalized Nanoparticles for Targeted Biosensing and Biological Applications', *ACS Omega*, 5(48), pp. 30767–30774.

Steinhauser, I., Spänkuch, B., Strebhardt, K. and Langer, K. (2006) 'Trastuzumab-modified nanoparticles: Optimisation of preparation and uptake in cancer cells', *Biomaterials*, 27(28), pp. 4975–4983.

Sung, Y.K. and Kim, S.W. (2020) 'Recent advances in polymeric drug delivery systems', *Biomaterials Research*, 24(1), p. 12.

Valabrega, G., Montemurro, F. and Aglietta, M. (2007) 'Trastuzumab: mechanism of action, resistance and future perspectives in HER2-overexpressing breast cancer', *Annals of Oncology*, 18(6), pp. 977–984.

Xie, W., Guo, Z., Gao, F., Gao, Q., Wang, D., Liaw, B., Cai, Q., Sun, X., Wang, X. and Zhao, L. (2018) 'Shape-, size- and structure-controlled synthesis and biocompatibility of iron oxide nanoparticles for magnetic theranostics', *Theranostics*, 8(12), pp. 3284–3307.

Yamada, Y. (2020) 'Dimerization of Doxorubicin Causes Its Precipitation', *ACS Omega*, 5(51), pp. 33235–33241.

Zhao, Y., Zheng, H., Wang, X., Zheng, X., Chen, Y., Fei, W., Zheng, Y., Wang, W. and Zheng, C. (2020) '<p>Enhanced Percutaneous Delivery of Methotrexate Using Micelles Prepared with Novel Cationic Amphipathic Material</p>', *International Journal of Nanomedicine*, Volume 15, pp. 3539–3550.